



universität
wien

MASTERARBEIT

Titel der Masterarbeit

„Detection of Ceria Nanoparticles
in Natural Soils using the Ce:La Ratio“

verfasst von

Willi Fabienke BSc

angestrebter akademischer Grad

Master of Science (MSc)

Wien, 2015

Studienkennzahl lt. Studienblatt: A 066 815

Studienrichtung lt. Studienblatt: Masterstudium Erdwissenschaften

Betreut von: Univ. Prof. Dr. Thilo Hofmann

Acknowledgements

During my work on this thesis I have not gathered most of the knowledge from experiments in the laboratory or analysis of data, but from the people I have been working with, who were willing to spend their time, sharing their own expertise and personal experience.

First I would like to thank Frank v. d. Kammer, who did not only provide countless ideas for even the most difficult problems, but also encouraged my scientific curiosity by giving me freedom in the choice of my topic as well as nearly unlimited access to the well equipped laboratories. I also want to thank Thilo Hofmann, for giving me the possibility to work in his group, which he leads excellently.

This thesis might have not been finished without the help of Antonia Praetorius, who was always open for discussion and successfully guided me through the final phase of my thesis. I want to thank Elisabeth Neubauer, who patiently taught me how to use the A4F in a very short time and Stephan Wagner, who showed me how to maintain the A4F in a functioning state in the following months, as often as it was necessary.

Wolfgang Obermaier taught me how to work efficiently in the lab, plan ahead of time and how important communication is to get things done as a team. Numerous discussions about the analysis of spICP-MS data with Jana Navratilova have helped me to understand the technique and its limitations. I would also like to thank Milica Velimirovic, Andreas Gondikas, Fazel Abdolapur Monikh and Daniela Moser for their helping hands. At this point I want to thank the whole Department of Environmental Geosciences group, which not only works well together scientifically, but also on a personal level.

The support of my family and friends, particularly during the difficult time at the end of the thesis, encouraged and motivated me to finish this important piece of work. Thank you, especially, Julia, Suse, and Kuno.

Contents

1	Abstract & Zusammenfassung	1
1.1	Abstract	1
1.2	Zusammenfassung	2
2	Introduction	3
3	Materials and Methods	6
3.1	Materials	6
3.2	Sampling	6
3.3	CeO ₂ Spiking Experiment	8
3.4	Sample Preparation	9
3.4.1	Aqueous colloid extraction	9
3.4.2	Sodium polytungstate colloid extraction	11
3.5	Instrumental Methods	14
3.5.1	Traditional ICP-MS and ICP-OES	14
3.5.2	Single Particle ICP-MS	14
3.5.3	Asymmetric Flow-FFF	15
3.6	Data Analysis	18
3.6.1	Single Particle ICP-MS	18
3.6.2	A4F fractionation quality control	19
3.6.3	A4F size calibration	19
3.6.4	A4F-ICP-MS mass spectra analysis	20
4	Results and Discussion	21
4.1	Sample Characterisation	21
4.1.1	Colloid extracts	21
4.1.2	Elemental composition of colloid extracts	23
4.1.3	La & Ce content in colloid extracts	23
4.1.4	Single Particle ICP-MS	26
4.2	CeO ₂ Spiking Experiment	27
4.2.1	CeO ₂ spiking suspensions	27

4.2.2	Ce recovery in spiked samples	29
4.2.3	Single particle ICP-MS of spiked colloid samples	31
4.2.4	A4F-ICP-MS coupling of spiked colloid samples	34
5	Conclusions and Outlook	40
6	Bibliography	43
7	Appendix	I
7.1	Abbreviations	I
7.2	Additional Tables and Figures	II
7.3	Eidesstattliche Erklärung	IX
7.4	Curriculum Vitae	X

1 Abstract & Zusammenfassung

1.1 Abstract

Engineered nanoparticles have found widespread applications over the last few years with many more in development (Kim et al. (2012), Edward and Spiros (2010), O'Brien and Cummins (2008)). Nanoparticles are interesting for many applications mainly because of their different chemical behaviour compared to the bulk material that they were made out of. CeO₂ nanoparticles (nCe) can be used as a diesel fuel additive, potentially exposing a broad population to nCe emissions. Engineered CeO₂ is different from natural Ce containing minerals, because of its purity and low La content. The ratio of Ce:La of 2.0:1 (± 0.2) is relatively stable in natural soils, due to the similar chemical behaviour of La & Ce. Higher ratios can indicate the presence of nCe and can also be used to quantify the amount of nCe in the sample (v. d. Kammer et al. (2013), Gantt et al. (2014)).

In this study Ce:La ratios of 2.0:1 (± 0.1) and 2.0:1 (± 0.2) were determined for natural soils and colloid suspensions extracted from those soils, respectively. An uncontaminated soil was spiked with different CeO₂ nanoparticle concentrations and colloid extracts were gained from those spiked soils to determine the detection limit for nCe using the Ce:La ratio. Detection of the spiked nCe in the colloid suspension at a concentration as low as 4.5% of the natural background (3.3 ppm Ce added to 73 ppm soil Ce-background) was possible using bulk element analysis via Inductively Coupled Plasma Mass Spectrometer (ICP-MS). Single particle ICP-MS showed to be a promising technique which might lower the detection limit by being more sensitive to shifts of the Ce:La ratio, but further method development is needed to prove this.

Coupling of a size separation technique (asymmetric flow field-flow fractionation) to an ICP-MS has shown that the spiked nCe probably attached to natural clay-mineral particles, giving information for future optimization of sample preparation techniques which might also lower the detection limit. In conclusion, this study shows that the Ce:La ratio can serve as a sensitive tool for the detection of technical CeO₂ nanoparticles in the environment.

1.2 Zusammenfassung

In den letzten Jahren wurden zahlreiche Anwendungen für synthetische Nanopartikel entdeckt, wobei viele weitere noch in der Entwicklung sind (Kim et al. (2012), Edward and Spiros (2010), O'Brien and Cummins (2008)). Nanopartikel sind insbesondere deshalb von Bedeutung, weil sich ihre chemischen Eigenschaften von denen des groben Ausgangsmaterials unterscheiden. Cerdioxid-Nanopartikel (nCe) können als Dieseldieselkraftstoffadditiv verwendet werden, wodurch potenziell eine breite Population dem Material ausgesetzt werden kann. Technische Cerium Nanopartikel unterscheiden sich von natürlichen Cer-Mineralen hauptsächlich durch ihren geringen Lanthan-Gehalt. Natürliche Böden weisen ein stabiles Ce:La-Verhältnis von 2.0:1 (± 0.2) auf, bedingt durch das sehr ähnliche chemische Verhalten von Lanthan und Cerium. Abweichungen von dem natürlichen Verhältnis weisen auf technische Cerium-Nanopartikel hin, deren Mengenkonzentrationen außerdem mit Hilfe des Ce:La-Verhältnisses geschätzt werden können (v. d. Kammer et al. (2013), Gantt et al. (2014)).

In dieser Arbeit wurden Ce:La-Verhältnisse von 2.0:1 (± 0.1) und 2.0:1 (± 0.2) für natürliche Böden bzw. Kolloidextrakte aus diesen Böden bestimmt. Eine natürlichen Bodenprobe wurden mit ansteigenden Konzentrationen von CeO₂ Nanopartikeln versetzt, um die Nachweisgrenze von nCe mit Hilfe des Ce:La-Verhältnisses zu ermitteln. In Kolloidextrakten dieser Proben, mit bekanntem natürlichen La- und Ce-Gehalt, konnte die Zugabe von nCe mit einem Massenäquivalent von 4.5% des natürlichen Ce-Hintergrundes (3.3 ppm nCe zu 73 ppm Hintergrund) durch Massenspektrometrie mit induktiv gekoppeltem Plasma (ICP-MS) detektiert werden. Erhöhte Sensitivität des Ce:La Verhältnisses könnte durch Einzelpartikelanalyse der Kolloidextrakte erreicht werden, allerdings benötigt es weiterer Methodenentwicklung um dies in der Praxis zu beweisen.

Analysen von Kolloidextrakten durch Kopplung einer nach Partikelgröße aufgelösten Elementaranalyse (Feld-Fluss-Fraktionierung gekoppelt mit Massenspektrometrie mit induktiv gekoppeltem Plasma) lassen vermuten, dass die zugegebenen, technischen CeO₂-Partikel wahrscheinlich mit natürlichen Tonmineralen Heteroaggregate bilden. Dieses Wissen kann für die Optimierung der Probenaufbereitung genutzt werden, um die Anreicherung technischer CeO₂-Nanopartikel zu bewirken und somit die Nachweisgrenze weiter nach unten zu verschieben. Diese Arbeit zeigt, dass das Ce:La-Verhältnis als empfindliches Werkzeug verwendet werden kann, um technische CeO₂-Nanopartikel in der Umwelt zu detektieren.

2 Introduction

Engineered nanoparticles (ENPs), defined here as man-made materials with at least one dimension <100 nm, have found widespread applications over the last few years with many more in development (Kim et al. (2012), Edward and Spiros (2010), O'Brien and Cummins (2008)). Nanoparticles are interesting for many applications mainly because of their different chemical behaviour compared to the bulk material that they were made out of. Advantages of the small sizes of nanoparticles include an increased reactivity due to their larger surface to volume ratio and increased transportability. Materials used for engineered nanoparticles are diverse, including carbon based materials (carbon nanotubes, fullerenes), metals (copper, gold) and metal oxides (Fe_2O_3 , Al_2O_3). Having many favourable properties, ENPs have found their way into more than 1500 consumer products (Project on Emerging Nanotechnologies, see <http://www.nanotechproject.org/cpi/products/>, accessed: 2 March 2015). Many of those products were introduced on the market by testing them with standard protocols, which are partly not suitable for nanoparticles, due to their different behaviour (v. d. Kammer and Neubauer, 2013). This entails the release of ENPs without detailed evaluation and understanding of their behaviour in the environment and their ecotoxicological effects (EPA, 2007). Once released into the environment, ENPs are difficult to detect, not only due to their low predicted concentrations in the ppt range, but also because of the common occurrence of similar natural nanoparticles (NNPs). This holds true for particles such as TiO_2 , Fe_2O_3 and SiO_2 , for which the differentiation between ENPs and NNPs proves to be difficult, even when there are promising approaches for the detection of those particles in environmental matrices, such as single particle inductively coupled mass spectrometry (SP-ICP-MS) for metal nanoparticles in water (Gondikas et al., 2014). For some applications ENPs have to be chemically pure compared to their naturally occurring equivalents, such as in chemical sensors or catalysts (Carpenter et al. (2012), Sun et al. (2012)). This difference in chemical composition might be used for the detection of the ENPs.

The rare earth element (REE) distribution in the earth's crust is relatively stable, despite some elements showing anomalies (Zdzisław and Agnieszka, 2015). This

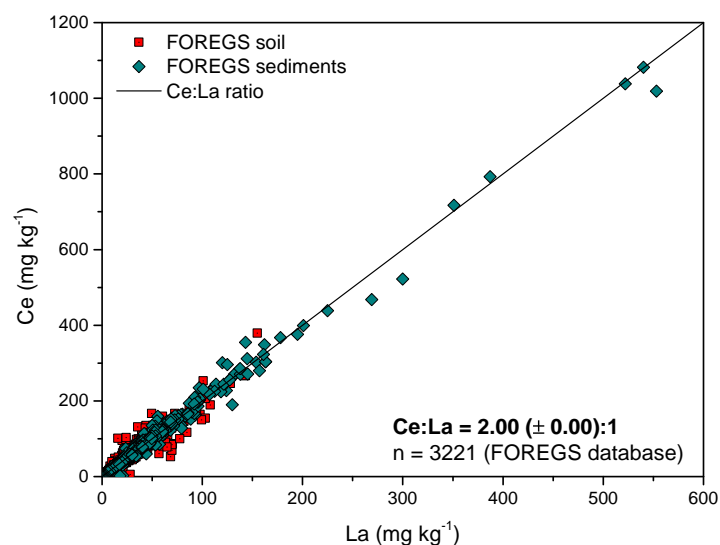


Figure 2.1: Cerium and lanthanum content of soils and sediments of the FOREGS database show a constant Ce:La ratio of 2.0:1. Figure adapted from v. d. Kammer et al. (2013).

also applies to the light rare earth elements La and Ce, which show a relative mass ratio of 2.0:1 (± 0.0) in soils and sediments as shown in Figure 2.1 (v. d. Kammer and Neubauer (2013)). Differing from natural Ce containing particles, technical CeO₂ nanoparticles (nCe) contain mainly Ce, with only traces of La. Deviations of the natural Ce:La ratio of 2:1 might be caused by the presence of nCe, shifting the ratio to higher values (v. d. Kammer et al., 2012). Gantt et al. (2014) have used the Ce:La ratio to distinguish between natural Ce containing particles and nCe in aerosols, successfully fitting their model to measured data. The emission source for nCe in that study were Stagecoach busses from the London bus fleet, which use diesel fuel additives containing nCe as a catalyst since 2003. Cerium based fuel additives are also currently used for public on-road vehicles in New Zealand (since 2005) and Canada (since 2010), as well as commercially available from Eolys (Rhodia Electronics & Catalysis), Envirox (Energenics Europe Limited), and Platinum Plus (Clean Diesel Technologies Incorporated). Although the use of nCe as a fuel additive is currently the only relevant source for environmental contamination, other future applications might cause further release of nCe into the environment. Other applications where nCe is used are photocatalysts, biomedical applications, polishing agents, coatings, cigarette additives and solid oxide fuel cells (Sun et al. (2012), Edward and Spiros (2010), Andersson et al. (2006)). Cassee et al. (2011) have reviewed the health and ecological effects of the use of nCe as a fuel additive and concluded that uncertainty remains and the topic requires additional research. Al-

though some time passed since that review, the toxicity of ceria nanoparticles is still not well understood, although recent studies have shown both bioaccumulation and health effects for different species (Collin et al. (2014), Gambardella et al. (2014)).

If nCe shows to have adverse health effects, detection of those particles in the environment will be important. In this work, the feasibility of the detection of nCe in natural soils and colloid extracts using the Ce:La ratio is evaluated. For development of our analytical approach on a well-defined system and evaluation of the detection limit of nCe in soils, this study was performed using natural soil samples spiked with known amounts of nCe (covering a wide range of concentrations). Additionally, uncontaminated soil samples were characterized in detail to provide a thorough assessment of background La and Ce concentrations. Aqueous colloid extracts were obtained from a selection of soil samples (natural and spiked) and analyzed for their Ce:La ratio using multiple techniques including SP-ICP-MS and particle size resolved mass analysis via coupling of Asymmetric Flow Field-flow fractionation to ICP-MS.

3 Materials and Methods

3.1 Materials

Ultra pure water ($<18.2 \text{ m}\Omega/\text{cm}$) was obtained from a Millipore Element apparatus (Millipore, Milford, MA, USA) and used throughout the work. ICP-MS calibration was done using PE Pure Plus Atomic Spectroscopy Standards (Norwalk, CT, USA). HNO_3 was bought from Merck (KGaA, Darmstadt Germany). NaCl, ammonium carbonate and ceria nanoparticles $<50 \text{ nm}$ were bought from Sigma Aldrich (St. Louis, MO, USA). Sources of other chemicals are described within the text.

3.2 Sampling

Soil samples for this study were taken at five sites in Vienna in 2014 (Figure 3.1). Four sampling locations representing natural CeO_2 uncontaminated soils were chosen within city parks. Those sampling locations were at least 200 m away from the next street to avoid potential CeO_2 NP contamination from diesel fuel additives. The fifth sampling location (WR) was an infiltration area of untreated road run-off of the Hadikgasse, which has a high traffic load from commuting (Figure 3.2). At each of the five locations three composite subsamples (WR: only two subsamples), with a minimum distance of 30 m to each other, were taken. Each composite subsample was blended from three equal parts taken within a radius of 2 m. Samples were taken with a clean metal shovel after removal of the first 1-3 cm of the topsoil, which has a high organic debris content. The composite soil samples were collected in plastic bags, closed air-tight and brought to the lab for storage at 4°C .

The five locations were given abbreviations, namely: Prater (PT), Pötzleinsdorfer Schlosspark (PS), Lainzer Tiergarten (LT), Stiftswald (SW) and Wienfluss-Radweg (WR). The subsamples of every location were identified by a numerical suffix (e.g.: PT1, PT2, PT3).

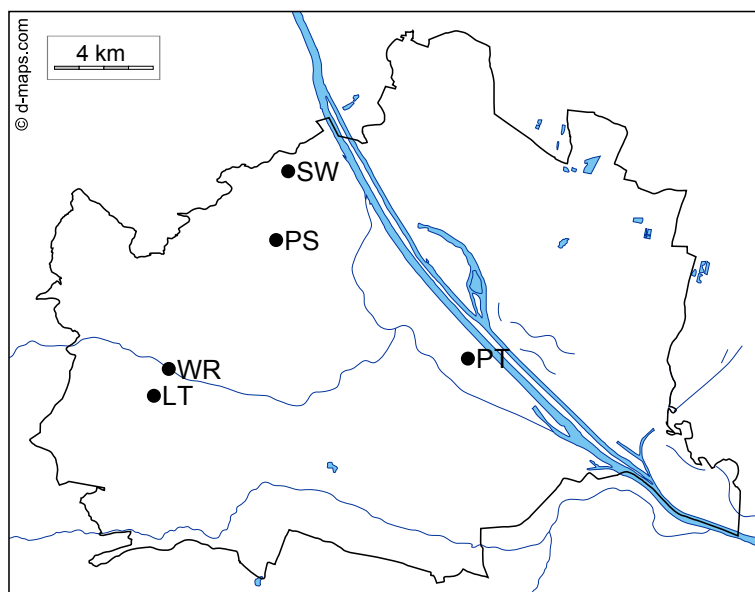


Figure 3.1: Map of Vienna showing the sampling locations: Prater (PT), Pötzleinsdorfer Schlosspark (PS), Lainzer Tiergarten (LT), Stiftswald (SW) and Wienfluss-Radweg (WR).



Figure 3.2: Soil samples WR1 & WR2 were taken from an infiltration area for road run-off of a heavily frequented commuter road.

3.3 CeO₂ Spiking Experiment

To determine the minimum concentration of technical CeO₂ nanoparticles needed for detection in a soil matrix, spiking experiments with nCe were conducted. Ceria nanoparticles used had a manufacturer stated diameter <50 nm and were suspended in ultra pure water. A homogeneous mixture of untreated soil of subsample PS3 was chosen for the spiking experiment, because an asymmetric flow field-flow fractionation method (a size separation technique described below) was already developed for PS3, a sample which had already been extracted for preliminary test. Seven spike suspensions were created for the spiking experiment. A blank containing no CeO₂ NPs will be referred to as spike suspension 0. The other six spike suspension had Ce contents from CeO₂ NPs of 3.3×10^{-4} to 33 mg, in steps of one order of magnitude, and will be referred to as spike suspensions 1–6, from lowest to highest concentration. Dry nCe powder was mixed with ultrapure water and sonicated in a bath (10 min, SONOREX SUPER RK 106, Bandelin, Berlin, Germany). The pure nCe powder in suspension had a positive zeta potential, which might have lead to particle losses due to absorption to negatively charged surfaces. The addition of Suwannee River Natural Organic Matter (SRNOM, final concentration 10 ppm TOC) to a 10 mg L⁻¹ nCe test suspension, which was not used for spiking, lead to a decrease of its zeta potential from +42.8 to -67.1 mV (Zetasizer Nano ZS, Malvern Instruments Ltd, UK), by coating the CeO₂ NPs with negatively charged NOM particles. The sonicated nCe stock suspensions were mixed with a SRNOM solution to give a total volume of 20 mL spiking suspensions with a final concentration of 10 ppm TOC. Zeta potential and z-average size measurements were done for all spiking suspensions. To decrease the particle size further, probe sonication (3 kJ, SONOPULS HD 3100, tip : TT13, Bandelin, Germany) of a nCe suspension (10 mg/L) was tested, but showed no significant decrease in z-average size compared to 10 min sonication in a bath (data not shown). Spike suspension 6 had an increased z-average size \varnothing of 800 nm compared to 280–330 nm of spiking suspensions 2–5, which was probably due to aggregation effects. It showed that spiking suspension 6 was not stable and sedimentation was visible after a rather short time (\sim 5 min), so it was applied onto the soil directly after sonication (see below). To each of seven 250 ml polymethylpentene (PMP) bottles (Nalgene, NY, USA) was added 100 g of homogenized soil (PS3) and 20 ml of the respective spiking suspension. The spiked soil samples of PS3 will be referred to as SPK0 to SPK6. All bottles were shaken manually until a homogeneous mixture formed (Figure 3.3), covered from light by aluminium foil and put on an overhead shaker overnight



Figure 3.3: Seven PMP bottles containing 100 g of soil spiked with 20 ml of CeO_2 nanoparticle suspension with various concentrations.

(20 rpm, REAX 20, Heidolph Instruments, Germany). The spiked soil samples were then treated like the other soil samples for extraction of their colloidal fractions (see below).

3.4 Sample Preparation

All soil samples were wet-sieved $<32\mu\text{m}$ with ultra pure water, frozen and freeze-dried. Samples PS1, PS2, PT1, PT2 and PT3 were wet-sieved with 100 ml water. For the other samples 200 to 300 ml were used, which resulted in much higher yields (e.g.: PS3 was wet-sieved twice with 100 ml and 250 ml which resulted in 24 and 37% of $<32\mu\text{m}$ dry mass, respectively). A portion of the wet-sieved and freeze-dried fractions of selected samples were digested for metal analysis with ICP-OES and ICP-MS.

3.4.1 Aqueous colloid extraction

Bearing in mind that Asymmetric Flow Field-Flow fractionation (AF4) is a technique well-suited for separation of particles suspended in aqueous media, an extraction method resulting in an aqueous colloid suspension is beneficial, as it minimizes the following sample preparation. An aqueous extraction method adapted from v. d. Kammer (2004) was used to create colloid suspensions from $<32\mu\text{m}$ soil fractions. For every sample, four grams of the freeze-dried $<32\mu\text{m}$ fraction was mixed with 40 ml of a 0.1M NaCl solution in a 50 ml centrifugation vial, shaken manually, protected from light with aluminium foil and put on a shaker for at least 21 h at 200 rpm (KS260 control, IKA, Staufen, Germany). This step was done to exchange divalent cations, which would later interfere with the colloid extraction

process due the increased coagulation effectiveness of two and three-valent cations on negative lyophobic colloids in comparison to monovalent cations (*Schulze-Hardy* rule, Nowicki and Nowicka (1994)). Due to the high ionic strength in the mixture, colloids were expected to be fully aggregated. The mixture was then centrifuged to give a 100 nm particle size cut-off for particles with a density of 2.6 g cm⁻³ (representing an average density for most relevant mineral phases, Beckett and Hart (1993)) using the following equation (Bernhardt, 1994):

$$t_s = \ln \left(\frac{r_{out}}{r_{in}} \right) \times \frac{18\eta}{4\pi^2 \Delta\rho d^2 \left(\frac{rpm}{60} \right)^2} \quad (3.1)$$

This equation assumes spherical particles and an increasing centrifugal force with the radius. It calculates the time, t_s , necessary for a particle with diameter d to travel from the surface of the sample (r_{in} , distance from rotor axis to sample surface) to a point beneath the surface (r_{out} , distance from motor axis to sampling point) under given revolutions per minute (rpm), density difference between particles and medium ($\Delta\rho$), and viscosity of the medium (η). This assures that after centrifugation all particles in the retrieved sample portion will be smaller than d . It must be noted that if the vial is filled with a homogeneous dispersion, also particles much smaller than d , starting below the surface and closer to r_{out} will be removed from the sample. The resulting size distribution is not representing the original distribution up to d . In this case r_{out} was set equal to the the distance from the rotor to the bottom of the vial. Since the particles were expected to be fully aggregated, the chosen cut-off of 100 nm under 4500 rpm was a suitable compromise between safe removal of all particles from the supernatant, centrifugation time and g-force related compaction of the sediment at the bottom of the tubes. Absence of particles in the supernatant was inspected visually by using a standard red laser pointer (clear supernatant, no scattered light visible to the naked eye at $\sim 30^\circ$ scattering angle). The supernatant of the spiked samples was collected for later analysis, but discarded for the natural samples. To the vials containing the sediments was added 35 ml of ultra pure water to reverse the aggregation induced by the high ionic strength by washing out the NaCl previously added. The sediments were then resuspended by vortexing (Vortex-Genie 2, Scientific Industries, NY, USA), bath sonicated (10 min), covered from light by a tinfoil layer, put on a shaker for at least 24 h and centrifuged again (as above). The supernatants returned turbid for all samples which stated the peptisation of the colloids.

The sediments were resuspended and centrifuged to give a 300 nm particle size cut-off. To limit the effect of changing the original size distribution (see above), the

maximum particle travelling distance was reduced by choosing r_{out} 20 ml below the sample surface (instead of 35 ml, the bottom of the vial). The top 20 ml of the supernatants were collected in 500 ml PMP bottles (Nalgene, NY, USA) and replaced with 20 ml of ultra pure water. The sediments in the vials were then bath sonicated (5 min), resuspended, put on a shaker for at least 1 h (200 rpm), bath sonicated again (10 min) and centrifuged to a particle-size cut-off of 300 nm. After collection of the supernatants (top 20 ml), the procedure was repeated until the supernatants returned substantially less turbid (Figure 3.4). The collected colloid suspensions were stored in the dark at 4 °C.

Preliminary Samples

An aqueous extraction similar to that described above was done for samples PT1, PT2, PT3, PS1, PS2 and PS3. This sample set was prepared slightly differently from the procedure described above, but changes are not described here because the final colloid extracts were not fully analyzed.

The aqueous extracts were obtained in May 2014 and A4F method optimization for the samples was begun, but not finalized. A4F method optimization was continued in October 2014, but by then the extracts had partially sedimented and aggregated. The aged colloid suspensions could not be fully resuspended by bath or probe sonication, which resulted in clogging issues during A4F pretests. To remove the aggregates from the colloid suspensions, the samples were centrifuged (particle size cut-off 150 and 300 nm) and further A4F test runs were conducted. However, the aged extracts showed a completely different elution behaviour than the fresh ones, which lead to the decision to prepare fresh colloidal extracts (see below).

Samples

The second extraction was done using natural samples PS2, LT1, LT2, the two road runoff samples WR1, WR2 and the spiked soil samples SPK0 to SPK6. For samples WR1 and WR2 only 3 g (instead of 4 g) of the freeze-dried <32µm fractions were used for the extraction, because of low yields of the <32µm sieving of 4.6 and 4.3 g, for WR1 and WR2, respectively.

3.4.2 Sodium polytungstate colloid extraction

Plathe et al. (2010) and v. d. Kammer (2004) have shown that colloid samples prepared with a similar aqueous extraction method were enriched in clays. This is

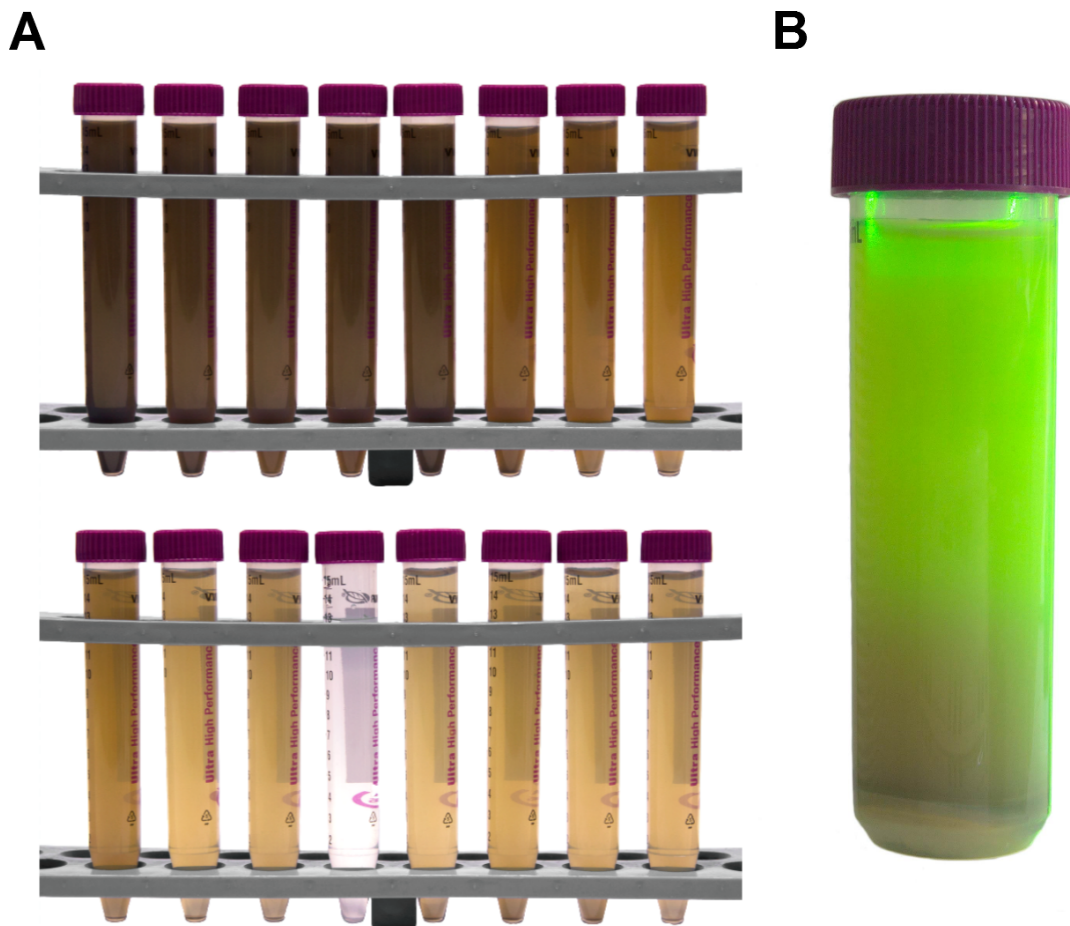


Figure 3.4: **A** Aqueous extracts of sample SPK0 from step 1 (top left) to step 16 (lower right). The decrease of turbidity shows a decrease of colloids extracted, step 12 is not shown. **B** Aqueous extract SPK0 before extraction step 17 (extract only collected until step 16) illuminated by a green laser pointer from the right. The sharp change of turbidity marks the maximum collection depth. The colloid suspension above that mark (containing only nanoparticles <300 nm assuming a density of 2.6 g cm^{-3}) was collected (see A).

because the effective sedimentation diameter of clay particles is larger than the diameter calculated by equation 3.1 (Jennings and Parslow (1988)) which leads to an enrichment of clay particles with sizes greater than the chosen cut-off in the acquired colloid extract. In addition to the enrichment of clays, heavier minerals such as Fe- and Mn-Oxides are depleted. Natural REE are often associated with high density Fe- and Mn-Oxides (Ohta and Kawabe (2000), Och et al. (2014)). This implies that aqueous colloid extracts gained with the protocol described above might be depleted of La and Ce. To increase the REE content of the extracts by removal of relatively light minerals, such as clays, a density separation colloid extraction protocol was adapted from Plathe et al. (2013) and applied to six samples (PS1, PS2, PS3, PT1, PT2 and PT3):

Ninety grams of LST Fastfloat (sodium heteropolytungstates dissolved in water, $\rho = 2.82 \text{ g mL}^{-1}$, Polytungstates Europe, UK) were mixed with 2.5 g of each sample ($<32 \text{ }\mu\text{m}$) in 90 mL centrifuge vials. The mixtures were shaken, bath sonicated (30 min) and centrifuged at 4500 rpm for 90 min. The light fraction and the supernatant of each sample were transferred into a new vial, bath sonicated (30 min) and centrifuged again. This process was repeated a 3rd time and the heavy fractions from all three runs were combined. Thirty millilitres of 0.1 M NaCl were added to each of the heavy fractions to exchange divalent cations (see above), bath sonicated for 10 min and centrifuged to a cut-off of 48 nm for particles with $\rho = 4 \text{ g cm}^{-3}$ (average density for metal oxides, (Plathe et al., 2010)). The supernatants were discarded and the sediments mixed again with 30 ml of 0.1 M NaCl. This NaCl washing routine was done 5 times in total for every heavy fraction.

The NaCl-washed sediments were mixed with 15 ml of ultra pure water, bath sonicated (5 min), put on a shaker (20 min) and centrifuged to a cut-off of 100 nm ($\rho = 4 \text{ g cm}^{-3}$). The supernatant came back clear for all six samples and no particles could be detected with a laser pointer. The supernatants were then discarded and replaced by 15 ml of ultra pure water. This was done seven times in total but no peptisation of colloids was observable. To test if bigger colloids were present in the sediments, the centrifugation step was repeated with a cut-off of 400 nm. The supernatants came back slightly turbid indicating the presence of particles in the size range of 100–400 nm. However, no extracts were collected and the aqueous extraction method (described above) was used instead.

3.5 Instrumental Methods

3.5.1 Traditional ICP-MS and ICP-OES

Portions of the <32 μm fractions of samples PT1–PT3, PS1–PS3, LT1, LT2, WR1, WR2 and SPK0–SPK6 were digested using a microwave (Multiwave 3000, PerkinElmer, MA, USA) of which dilutions were analyzed using ICP-OES (Optima 5300 DL, PerkinElmer, MA, USA) and ICP-MS (7700x ICP-MS, Agilent Technologies, CA, USA) for multiple elements. The colloidal extracts (PS2, LT1, LT2, WR1, WR2, SPK0–SPK6) were diluted and analyzed without digestion using ICP-OES and ICP-MS.

3.5.2 Single Particle ICP-MS

Single particle inductively coupled plasma mass spectrometry (SP-ICP-MS) is a relatively new technique for counting, determination of masses and sizing of nanoparticles. Degueldre and Favarger (2003) introduced the technique for colloid analysis and describe in detail the theory behind the particle characterization, so only a short overview of the technique will be given here. The idea of SP-ICP-MS is to monitor a single element of a highly diluted sample in time resolved analysis mode (TRA, also single particle mode), achieving that mass information of the monitored element can be recorded typically every 5–20 ms. The constant low background signal during the TRA measurement is made up of the dissolved elemental contribution as well as the instrument background. If a single particle, containing the element monitored, is ionized in the plasma, a sharp peak can be observed in the mass spectrum. Frequency and height of the peaks can be used to calculate particle number concentrations and particle masses. If the particle stoichiometry, density and shape are known (or assumed), particle sizes can be calculated. To allow proper statistical analysis, samples should be diluted so that particles make up 1–5% of the measured data points (Pace et al., 2011). For this study, SP-ICP-MS data for La and Ce were gained by measuring highly diluted colloidal samples in TRA mode on a 7700x ICP-MS (Agilent Technologies, CA, USA). Multiple dilutions in steps of one order of magnitude were measured for every sample. The sample introduction system consisted of a borosilicate glass MicroMist nebulizer and a quartz spray chamber (Agilent Technologies, CA, USA). The sample uptake rate was measured with a TruFlo sample monitor (Glass Expansion, Australia). Default instrumental and data acquisition parameters are listed in Table 3.1. Instrument tuning was done on a daily basis to ensure maximum signal response.

Instrumental parameters	
RF power	1550 W
Argon gas flow rate	
Carrier	0.8 L min ⁻¹
Dilution	0.4 L min ⁻¹
He cell gas flow rate	4.5 mL min ⁻¹
Sample uptake rate	0.344 mL min ⁻¹
Data acquisition parameters	
Isotopes monitored	¹⁴⁰ La, ¹³⁹ Ce
Dwell time	5 ms
Total acquisition time	120 s

Table 3.1: Default instrumental and data acquisition parameters for single particle ICP-MS

Calibration of dissolved La, Ce and Au was done daily prior to sample analysis by measuring eight dissolved standards per element with concentrations ranging from 0 to 50 µg mL⁻¹. To determine the estimated transport efficiency (ETA) on a daily basis, which is needed for calculation of particle sizes, a Au nanoparticle standard with a nominal diameter of 60 nm (BBI Solutions, Cardiff, UK) was measured in TRA mode in triplicate.

A selection of 12 samples was analyzed: natural samples PS2, LT1, LT2 and spike blank SPK0, road run-off samples WR1 and WR2 and the spiked samples SPK1–SPK6.

3.5.3 Asymmetric Flow-FFF

Asymmetric Flow Field-Flow fractionation (A4F) is a particle size separation technique for aqueous suspensions with sizes ranging from 1 nm to 1 µm (Beckett and Hart (1993), v. d. Kammer et al. (2005)) and is one of the least invasive high resolution separation methods currently available.

The sample is introduced into a flat (50–350 µm), elongated channel having an in- and outlet for a carrier liquid and a porous frit at the bottom of the channel on which a membrane (usually 5–100 kDa cut-off) is installed (Figure 3.5). A carrier liquid is pumped through the channel of which a part is being removed through the membrane at the bottom (cross flow, XF), applying a field to the particles perpendicular to the flow of the carrier liquid. This field moves particles towards the bottom of the channel. The diffusion of the particles is working against this field,

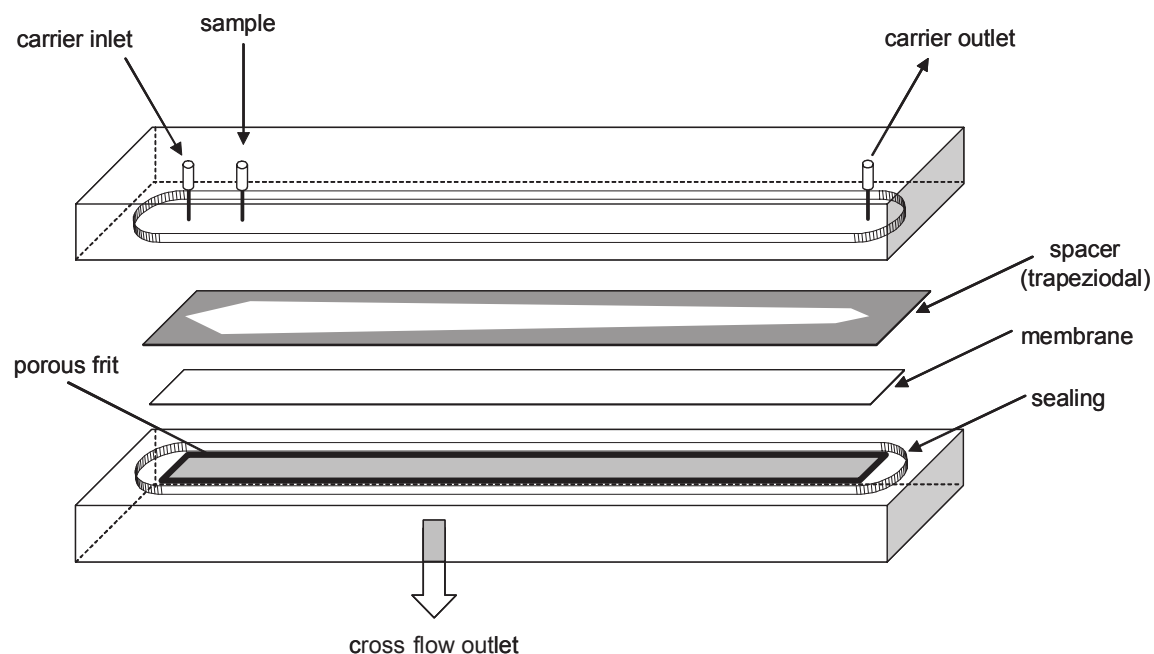


Figure 3.5: Schematic representation of an asymmetric Flow-FFF channel. Figure adapted from v. d. Kammer (2004).

moving them away from the bottom of the channel. Small particles have a greater diffusion coefficient than bigger ones (v. d. Kammer, 2004), resulting in a continuous vertical size distribution in the channel with the biggest particles being closest and the smallest particles being furthest away from the membrane. The laminar flow profile in a flat channel is parabolic, which involves a maximum velocity of the carrier in the middle of the channel and a reduction to zero at the channel walls. This results in an earlier elution of smaller particles, which are positioned towards the center of the channel, and a later elution of larger particles, being closer to the bottom of the channel. The retention and resolution of the A4F size separation depend mainly on the cross flow rate as well as the electrostatic properties of the particles, the latter being alterable by different carrier liquid compositions (Ionic strength, pH, surfactants). Higher charged particles can elute too early because of repulsion from the membrane by electrostatic interactions which results in non ideal separation. The ionic strength of the carrier has to be precisely controlled to limit those interferences. High cross flows, leading to better resolution, can cause irreversible attachment of particles to the membrane during focussing and during the run, which results in a selective loss of the biggest particles. For quantification of that loss, a recovery run can be done under similar conditions as a regular separation run but with the following changes: the sample is introduced into the channel without focusing and no cross flow is applied during the run. The recovery (Rec, in

%) can be calculated according to the following formula:

$$Rec = \frac{\int_{t_1}^{t_2} I_s dt V_s^{-1}}{\int I_r dt V_r^{-1}} \quad (3.2)$$

Where I_s is the signal intensity of the sample run, t is the time, t_1 and t_2 are the beginning and the end of the elution of the sample peak, respectively, V_s is the volume of the sample, I_r is the signal intensity of the recovery run and V_r is the volume of the recovery. To convert the elution time to a particle size, different approaches can be used: FFF-theory or calibration with polystyrol size standards. The outlet of the channel can be coupled to various detectors for online sample characterization or can be collected for later analysis.

Asymmetric Flow-FFF setup

An Eclipse 3+ A4F separation system (Wyatt Technologies, CA, USA) connected to a long channel (LC, 275mm tip to tip length, 350 μ m spacer, Wyatt Technologies, CA, USA) was used in this study. The membrane used was a 10 kDa regenerated cellulose membrane (Millipore, MA, USA) and changed approximately every 30 runs. For run condition optimization the system was coupled online to a multi-angle laser light scattering (MALLS) detector (HELEOS II, Wyatt Technologies, CA, USA) which was used to determine the radius of gyration (r_g). Samples were injected using an autosampler (Agilent Technologies 1200 Series). Carrier liquid was mixed online by an Agilent Technologies 1200 Series quaternary pump equipped with a micro-vacuum degasser. Ultra pure water used for online-mixing of the carrier liquid was held bacteria free by a UV-lamp.

Asymmetric Flow-FFF run condition optimization

An A4F method by Neubauer et al. (2013) was used as a starting point for method development. The detector flow rate (DF) was always set to 1 mL min⁻¹ for ease of converting min to mL. Different cross flows (0.35–0.75 mL min⁻¹) and ammonium carbonate concentrations (0.05–0.3 mM) were tested, resulting in either low resolution or low sample recoveries. The final method used is described in Table 3.2. To validate the method, a stable colloid sample regularly used as an in-house reference (Meisterjahn et al. (2014), Plathe et al. (2010)) was analyzed by MALLS and compared to previous results.

Multiple runs of one sample under the same conditions had shown that the recovery calculated with equation 3.2 dropped slightly for every consecutive run (data

Asymmetric Flow-FFF run parameters	
Carrier composition	0.15 mM ammonium carbonate
Carrier pH	7.4
Injection volume	50 μL
Focus flow rate	0.6 mL min^{-1}
Focus time	10 min
Detector flow rate	1 mL min^{-1}
Cross flow rate	0.6 mL min^{-1}
Sample run time	80 min
Recovery run time	12 min

Table 3.2: Asymmetric Flow-FFF run parameters.

not shown). This was thought to be due to sedimentation of the sample. To address this problem, an injector program was written which mixes the sample by drawing and reinjecting 100 μL of the sample into the vial three times prior to sample uptake and injection. This helped to reduce the drop of recovery of multiple injections (data not shown).

Asymmetric Flow-FFF coupled to ICP-MS

Five samples from the CeO_2 spiking experiment (SPK0, SPK3, SPK4, SPK5, SPK6) were analyzed for size resolved elemental composition by coupling A4F with an ICP-MS using the A4F-method described in Table 3.2. After leaving the MALLS detector the flow was split, reducing the flow rate entering the ICP-MS from 1 mL min^{-1} to $\sim 0.34 \text{ mL min}^{-1}$. Size resolved elemental concentrations of the the following isotopes were monitored: ^{27}Al , ^{48}Ti , ^{55}Mn , ^{56}Fe , ^{63}Cu , ^{64}Zn , ^{139}La , ^{140}Ce , ^{146}Nd , ^{157}Gd , ^{208}Pb and ^{232}Th . Calibration was done using eight multi element standards of the elements listed above stabilized in 0.5 M subboiled HNO_3 .

3.6 Data Analysis

3.6.1 Single Particle ICP-MS

For proper counting and sizing of nanoparticles via SP-ICP-MS, the estimated transport efficiency (ETA) is needed (Pace et al., 2011). The ETA was determined by analysis of the 60 nm Au particle data using two different approaches: the particle size method and the particle frequency method. Detailed description of the methods can be found in Pace et al. (2011). The dissolved Au-calibration, which is needed for the particle size approach, was created using standards from 0 to 2.5 $\mu\text{g L}^{-1}$,

which covers the signal response of the 60 nm particles. The particle cut-off was chosen manually at 10,000 counts per second (CPS) which resulted in a Gaussian shaped size distribution needed for the particle size method. The dissolved calibration curves for La and Ce were created using standards from 0 to 2.5 $\mu\text{g L}^{-1}$, which covered the range of most single particle events registered.

Sample data was first treated by calculation of the corresponding masses for the counts registered resulting in mass vs time fractograms. Single particle mass cut-offs were determined for La for each sample, separating particle events from the background. To directly compare the results of La & Ce, the cut-off for Ce was set $2 \times$ the cut-off of La, because of the assumption that in every particle there is twice the mass of Ce as of La. Particle number concentrations and particle mass concentrations were calculated for the stock colloid suspensions, taking into account the dilution, sample flow rate and ETA. Apparent CeO_2 diameters (d) were calculated for the Ce particle events assuming spherical geometry and using the following equation:

$$d = \sqrt[3]{\frac{6 \times m_p}{\pi \times \rho}} \quad (3.3)$$

Where m_p is the mass of a particle event, and ρ is the particle density (7.65 g cm^{-3} , Zagaynov and Kutsev (2014)). Size distribution histograms for apparent CeO_2 diameters were calculated for the spiked samples SPK0 to SPK6.

3.6.2 A4F fractionation quality control

The separation by A4F was evaluated by calculated radius of gyration (r_g) values from MALLS analysis (v. d. Kammer et al. (2005), Baalousha et al. (2006)). The r_g values were determined by fitting the Rayleigh ratios of the sample peaks obtained at different scattering angles with a 1st order Zimm fit (v. d. Kammer et al., 2005), using ASTRA 5.4 software (Wyatt Technology, Dernbach, Germany).

3.6.3 A4F size calibration

Conversion of elution volume of a A4F separation run to particle size can be done using different approaches (e.g.: FFF-theory, polysterol size standards(PSS)). A PSS calibration could not be done for the used channel and FFF run conditions, because of problems with non-reproducible PSS runs, which could not be solved within the time frame of this study. Size calibration using FFF-theory can differ from the real separation process in the channel due to irregular membrane swelling, reducing

the nominal spacer distance of the channel and therefore changing the separation (v. d. Kammer, 2004). Because the membrane used was known to swell, calibration using FFF-theory would have been inaccurate. As a workaround, size calibration was done using a stable colloid sample (Ref6) which is often used as an in-house reference sample. In-house data (unpublished) for a PSS calibrated separation run of Ref6 was used to calibrate the runs in this study. For this, the r_g values for the calibrated Ref6 run were fitted using linear regression, resulting in an equation transforming r_g values into hydrodynamic diameters. The calculated Radius of gyration values for the Ref6 run of this study were fitted using linear regression analysis, transforming elution volume into r_g . The combination of those two functions convert the elution volume from runs in the uncalibrated channel into a PSS-calibrated hydrodynamic diameter.

3.6.4 A4F-ICP-MS mass spectra analysis

The size resolved mass spectra obtained for the spiked samples were converted from counts to concentrations using a linear calibration for each element. The calibration curves were calculated using MassHunter Offline Analysis (Agilent Technologies, CA, USA). For some elements, the HNO_3 used for acidification of the dissolved elemental standards added a significant background (e.g.: Cu, Zn), while for other elements the carrier liquid used for A4F separation had a higher dissolved content (e.g.: Al, Nd, Th). This effect was corrected by setting the intersect of the calibration curves equal to the average element response of the carrier liquid. Data processing of the obtained .csv files from MALLS and ICP-MS was done using OriginPro 9.0 (OriginLab, Northampton, MA, USA). The 90° MALLS fractogram of every sample was analyzed for the void peak, which states the beginning of the elution with the release of the unfocused sample from the channel. This void volume was subtracted from the total elution volume to give the size separated elution volume. The subtracted elution volumes were then converted into hydrodynamic diameters (see above). The time-values of the time resolved ICP-MS mass spectra were converted into elution volume by division of the time through the detector flow of the A4F and subtraction of the void peak volume determined by MALLS analysis. In addition, the volume from the tubing between the MALLS detector and the ICP-MS was subtracted. Spectra of Al and Fe were smoothed using a Fast Fourier Transform smoothing filter (20 points, cut-off frequency: auto), La and Ce spectra were smoothed using an Adjacent-Averaging algorithm (130 points, weighted average).

4 Results and Discussion

4.1 Sample Characterisation

4.1.1 Colloid extracts

The extracts of the environmental samples PS2, LT1 and the spiked samples SPK1–SPK6 had a brown colour similar to that of SPK0 (see Figure 3.4) which was probably due to the high clay content. Both road run-off extracts (WR1, WR2) as well as the soil extract LT2 had a distinct dark grey color. As shown in Table 4.2, the $<32\mu\text{m}$ fractions of WR1 and WR2 had a high loss on ignition (LOI), which might be due to soot or tire abrasion, also causing the dark colour of the extracts.

Suspended colloidal matter (SCM) concentrations, determined by weighing of 20 nm filtrates, were between 2500 and 2600 mgL^{-1} for spiked samples SPK0–SPK2. For the samples SPK3–SPK6 the SCM concentrations determined (1600–1700 mgL^{-1}) were far below those of SPK0–SPK2, although the source material was the same. This trend could not be seen in the Al, Fe and Si concentrations of the respective colloid extracts determined by ICP-MS and ICP-OES (Appendix Table 7.4). Also simplified mass balances, as a sum of Al_2O_3 , SiO_2 and Fe_2O_3 , of the colloid extracts SPK3–SPK6 were above 100% using the SCM concentration determined by 20 nm filtration which is a clear indication that the SCM concentrations for SPK3–SPK6 were determined wrongly.

For further calculations of colloid mass based element contents, the SCM concentrations for SPK3–SPK6 were approximated as the average of the SCM concentrations of SPK0–SPK2. This assumption might be faulty if the spiked CeO_2 NPs changed the colloidal suspension behaviour, although similar Al, Fe and Si concentrations of the colloid suspensions SPK0–SPK6 suggest that this might not be the case. A repetition of the 20 nm filtration of the colloid extracts would have solved this open question, but was not done due to time constraints.

The pH values of the colloid extracts, shown in Table 4.1, were in a neutral range from 6.4 to 7.2 for most samples, except for LT2 having a pH of 5.3.

Colloid extraction yields were in the range of 3.5–29% and were calculated from the amount of suspended colloidal matter extracted from the <32µm fractions. Brown coloured extracts (PS2, LT2, SPK0–SPK6) had a higher yield than black coloured extracts (WR1, WR2, LT2) with 18–29% and 3.5–7.4%, respectively. The brown colour of the extracts probably originated from a high clay content, which is enriched during the extraction process. The lowest extraction yields were determined for the road run-off samples WR1 and WR2 with 6.0 and 3.5%, respectively. High concentrations of tire wear particles might be a contributing factor to the low extraction yields, because their mean diameter is in the size range of 10–20 µm (Councell et al., 2004), entailing in sedimentation of those big particles during centrifugation. Another contributing factor might be that soot particles suspended in the colloid extracts, having a particle size of ~10 nm (Karjalainen et al., 2014), simply go through the 20 nm filter used for SCM determination. Extraction yields determined do not represent the total extractable colloidal fraction, because further extraction steps would have increased the extracted SCM mass of every sample.

Sample	<32µm fraction (%)	SCM (mg L ⁻¹)	SCM yield (%)	colloid pH
LT1	23	2500	18	6.8
LT2	7.6	920	7.4	5.3
WR1	4.6	570	6.0	7.2
WR2	4.3	330	3.5	7.2
PS2	10	3600	29	7.2
SPK0	36	2600	21	6.6
SPK1	37	2500	20	6.6
SPK2	39	2500	20	6.5
SPK3	38	1700	13	6.5
SPK4	41	1600	13	6.5
SPK5	38	1600	13	6.4
SPK6	38	1700	14	6.4

Table 4.1: Fraction <32µm of soils after wet sieving, suspended colloidal matter (SCM) of aqueous extracts determined by filtration (20 nm filter) and pH values of colloid extracts. SCM extraction yields state the mass percentage of colloids extracted from <32µm fractions. SCM content for samples SPK3–SPK6 did not match the total concentrations of major elements.

Sodium polytungstate colloid extraction

To increase the amount of Fe- and Mn-oxides in the colloid suspension, which are possible REE hosts but selectively depleted during centrifugation, a sodium poly-

tungstate colloid extraction method was applied to six different samples (PT1, PT2, PT3, PS1, PS2, PS3). The extracts centrifuged to a particle cut-off of 400 nm ($\rho = 4 \text{ g cm}^{-3}$) were only slightly turbid, indicating a low particle concentration. Extracts gained by centrifugation for a cut-off of 100 nm were totally clear and particle free by inspection with a laser pointer. It is possible that the $<32\mu\text{m}$ fractions used for the extraction had very little particles with a density $>2.6 \text{ g cm}^{-3}$ in the size range of 100 nm \varnothing , but it is not very likely. A possible reason for the low extraction efficiency might be precipitation of scheelite (CaWO_4 , Atademir et al. (1979)) in the $<32\mu\text{m}$ fractions, which could keep other particles from resuspending by cementing them. To test this hypothesis, removal of soluble Ca-bearing minerals in the $<32\mu\text{m}$ fractions prior to mixing with sodium polytungstate solution could be done. Plathe (2010) has successfully extracted metal oxide nanoparticles from river sediments using a similar method which leaves the question open why the approach did not work in this study. As the sodium polytungstate colloid extraction might push the detection limits of high density metals in colloid extracts even lower, further experiments and method optimization are promising.

4.1.2 Elemental composition of colloid extracts

In Table 4.2 the main elements of the $<32 \mu\text{m}$ fraction and colloid extracts are shown. The enrichment factor (EF) is the relative enrichment of the element in the colloid fraction compared to the $<32 \mu\text{m}$ fraction. The enrichment factors for Al_2O_3 from 1.5 to 2.0 indicate an enrichment of clays, which is consistent with oblate shaped particles having a greater equivalent sedimentation diameter than spherical particles and therefore enriching during centrifugation. SiO_2 enrichment factors from 0.83 to 1.3 show no changes in relative Si content for all samples, except for LT2, having an EF of 0.66 for SiO_2 . For Fe_2O_3 the enrichment factors follow the trend of Al_2O_3 , indicating that the main source of Fe is from particles enriched in the colloid suspension, e.g. clays.

4.1.3 La & Ce content in colloid extracts

Cerium and lanthanum concentrations of the digested $<32\mu\text{m}$ fractions and the colloid extracts were determined by ICP-MS and are shown in Table 4.3. Only the natural samples, including spike blank SPK0, and the road run-off samples will be described here, the spiked samples SPK1–SPK6 will be discussed separately below. The REE content of $<32\mu\text{m}$ fractions the unspiked samples were within a range of 16 to 38 ppm and 34 to 79 ppm for La and Ce, respectively. Similar concentra-

Sample	Al ₂ O ₃			SiO ₂			Fe ₂ O ₃			LOI
	<32µm (%)	coll (%)	EF	<32µm (%)	coll (%)	EF	<32µm (%)	coll (%)	EF	<32µm (%)
LT1	13	26	2.0	59	56	0.95	4.0	7.5	1.9	15
LT2	14	21	1.5	60	40	0.66	3.5	8.6	2.4	13
WR1	8.1	14	1.7	31	36	1.2	7.7	9.1	1.2	32
WR2	7.4	15	2.0	26	35	1.3	7.7	10	1.4	33
PS2	16	23	1.4	45	48	1.1	5.3	6.4	1.2	19
SPK0	15	27	1.8	58	55	0.94	5.2	10	2.0	12
SPK1	15	28	1.8	61	56	0.93	5.2	11	2.1	12
SPK2	14	26	1.8	61	54	0.89	4.8	9.8	2.1	12
SPK3	15	23	1.5	61	51	0.83	4.8	8.9	1.8	11
SPK4	15	25	1.7	59	53	0.89	5.1	10	1.9	11
SPK5	15	25	1.7	60	51	0.85	5.0	10	1.9	12
SPK6	15	25	1.7	43	52	1.2	5.0	10	1.9	12

Table 4.2: Main element composition for <32 µm fractions and colloid suspensions (coll) as determined by ICP-MS (Al, Fe) and ICP-OES (Si). The colloid enrichment factor (EF) is the relative enrichment of the element in the colloid fraction compared to the <32µm fraction. Loss on ignition (LOI) was determined at 1000°C.

tions were reported for top soils in Europe as well as soils in south china (Zdzisław and Agnieszka, 2015). The colloid enrichment factors for La and Ce show similar trends, indicating that there is no selective fractionation process for either of the elements. Colloidal sample LT2 has enrichment factors of 0.25 and 0.30 for La and Ce, respectively. Those low enrichment factors might be due to selective loss of REE hosting Fe- and Mn-oxides during centrifugation (see section 3.4.1). Ratios of Ce:La for the <32µm fractions as well as the colloid suspensions vary between 1.8 and 2.4 and are within the range for soils and stream sediments reported by v. d. Kammer and Neubauer (2013). This shows that the Ce:La ratio does not change significantly during the colloidal extraction process for the samples analyzed, which is a key requirement for the detection of CeO₂ NPs by the Ce:La ratio. The highest Ce:La ratios were 2.4, 2.3 and 2.5 for the colloid suspensions of LT2, WR1 and WR2, respectively. Those were also the colloid suspensions with the lowest overall suspended colloidal matter concentrations and therefore the lowest La and Ce concentrations in the colloid suspensions analyzed. The La and Ce concentrations measured for LT2, WR1 and WR2 were close to the detection limit and therefore might have a greater error than the other samples, measured at higher concentrations. Measuring at higher concentrations would have limited those errors, but was not done to limit the amount of carbon deposition on the ICP-MS cone.

Sample	La			Ce			Ce:La ratio	
	<32 μ m (ppm)	coll (ppm)	EF	<32 μ m (ppm)	coll (ppm)	EF	<32 μ m	coll
LT1	30	20	0.68	56	36	0.64	1.9	1.8
LT2	39	10	0.25	79	24	0.30	2.0	2.4
WR1	18	17	1.0	38	39	1.0	2.1	2.3
WR2	16	15	0.92	34	38	1.1	2.1	2.5
PS2	30	21	0.69	62	42	0.67	2.0	2.0
SPK0	36	27	0.76	73	55	0.75	2.0	2.0
SPK1	36	29	0.79	74	59	0.80	2.0	2.1
SPK2	34	25	0.73	72	53	0.75	2.1	2.1
SPK3	35	23	0.65	74	46	0.62	2.1	2.0
SPK4	37	24	0.63	79	59	0.75	2.1	2.5
SPK5	35	23	0.65	130	150	1.2	3.7	6.6
SPK6	35	25	0.71	610	1000	1.6	17	40

Table 4.3: Summary of La and Ce content in the <32 μ m fractions and colloid suspensions (coll). The colloid enrichment factor (EF) is the relative enrichment of the element in the colloid fraction compared to the <32 μ m fraction.

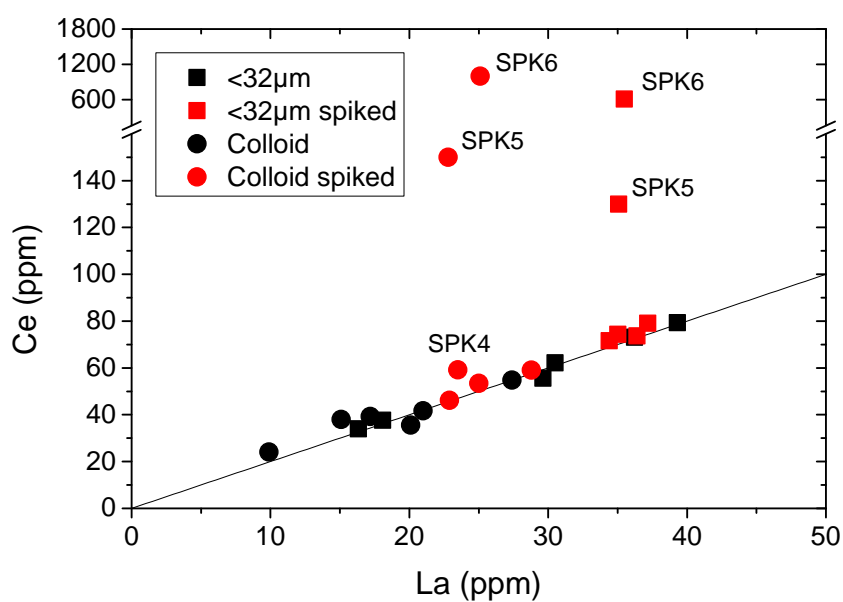


Figure 4.1: La and Ce concentrations of environmental samples in <32 μ m fractions and colloid extracts measured by ICP-MS. The Ce and La concentrations for the colloidal extracts are given within the suspended colloidal matter, not the aqueous phase. The theoretical Ce:La ratio for uncontaminated samples of 2:1 is shown as a solid line.

4.1.4 Single Particle ICP-MS

Single particle ICP-MS (SP-ICP-MS) data for La and Ce were gained by measuring highly diluted colloidal samples in time resolved analysis mode on an ICP-MS. The estimated transport efficiency (ETA) was determined by analysis of a 60 nm Au standard to enable the conversion of raw data signals to particle masses and particle sizes. The ETA determined by particle size and by particle number concentration were 4.0 and 5.7%, respectively. Calculation of the ETA using the size method, which fits the average signal of registered Au NP events to the known standard size, assumes a Gaussian size distribution of the standard. If the size of the Au size standard used is not Gaussian distributed, wrong transport efficiencies are calculated. The dissolved Au calibration needed for the size method is another source of inaccuracy. Using the particle frequency method, which only compares the amount of registered NP pulses to the known particle number concentration of the Au size standard, eliminates those factors. However, for the accuracy of the particle number method it is crucial that the Au particle standard used is well described. Because the Au particle standard used for ETA determination was a fresh stock, the ETA of 5.7% calculated by particle number concentration was used for further calculations. The difference of 30% in ETA compared to the particle size method is big for the determination of particle masses, but when masses are converted to particle sizes, the difference reduces to 8%.

Single particle measurements of La and Ce were done on two different days using freshly prepared diluted samples, which might have been slightly different in composition due to aging of the colloid suspensions. For even better comparability of La and Ce results, both measurements could have been done on the same day with the very same diluted samples. Only the natural samples, including spike blank SPK0, and the road run-off samples will be described here, the spiked samples SPK1–SPK6 will be discussed separately below.

Particles were detected above a cut-off of 0.1 and 0.2 fg for La and Ce, respectively. Ce-containing particles with Ce masses smaller than 0.2 fg could have been analyzed for most samples, but were excluded for a direct comparison of Ce and La particle number concentrations (see section 3.6.1). Accurate determination of small particles with masses producing a signal close to the background needs the application of rather complicated statistical methods, e.g.: background subtraction (Laborda et al., 2013). Because a rather simple approach for the distinction of particles from background was used, some of the smallest particles determined might be false positives. To limit the amount of false positive particle counts, the cut-offs

for La were chosen relatively high, meaning that events below the cut-off might still have been particle events, but were considered as background. The resulting cut-off of 0.2 fg for Ce equals a CeO₂ diameter of 40 nm.

The relative abundance of detected particle events were 1.0–2.5% and 1.0–2.4% for La and Ce, respectively, which is within the optimum range of 1–5% for single particle analysis (Pace et al., 2011). Ratios of Ce:La of the particle number concentrations varied between 0.98 and 1.4, showing that there were roughly equal Ce and La containing particles in the samples. For samples WR1, WR2 and LT2, which also had a dark grey colour, the maximum Ce signals were significantly higher than $2 \times$ the La signal (Appendix Figure 7.2), which might indicate the presence of minerals containing more Ce than La, possibly being nCe. Identification of such particles would be possible by analysis of the extracted colloids using transmission electron microscopy combined with energy-dispersive X-ray spectroscopy.

Single particle mass concentrations for La and Ce are shown in Graph 4.2. Particle mass concentrations for La and Ce show a similar trend as the suspended colloidal matter concentrations, with LT2, WR1 and WR2 having the lowest concentrations. The colloidal particle mass ratios for Ce:La varied between 1.8 and 3.0. The minimum Ce:La ratio of 1.8 of WR2 shows that a small number of relatively big Ce-containing particle events does not have to be visible in the Ce:La ratio, keeping in mind that WR1 showed some of the biggest Ce single particle events. CeO₂ size distributions for all environmental samples were similar with average apparent CeO₂ diameters in the range of 51–58 nm. The average particle mass ratio for Ce:La in natural samples is less stable than the Ce:La ratios within the bulk colloid suspensions with 2.3 (± 0.4) and 2.0 (± 0.2), respectively. Further single particle measurements, including replicates and longer acquisition times, are needed to determine if the Ce:La ratio really varies between the bulk colloid and the single particle level of those samples, or if the differences in this sample set are due to statistical errors of the single particle analysis. Although there is still room for improvement of the experimental setup, the relatively stable Ce:La ratios support the hypothesis that high ratios might be used for detection of nCe using SP-ICP-MS.

4.2 CeO₂ Spiking Experiment

4.2.1 CeO₂ spiking suspensions

Zeta potential and Z-average sizes were determined for the CeO₂ nanoparticle suspensions used to spike the soil samples prior to colloid extraction. Unstabilized

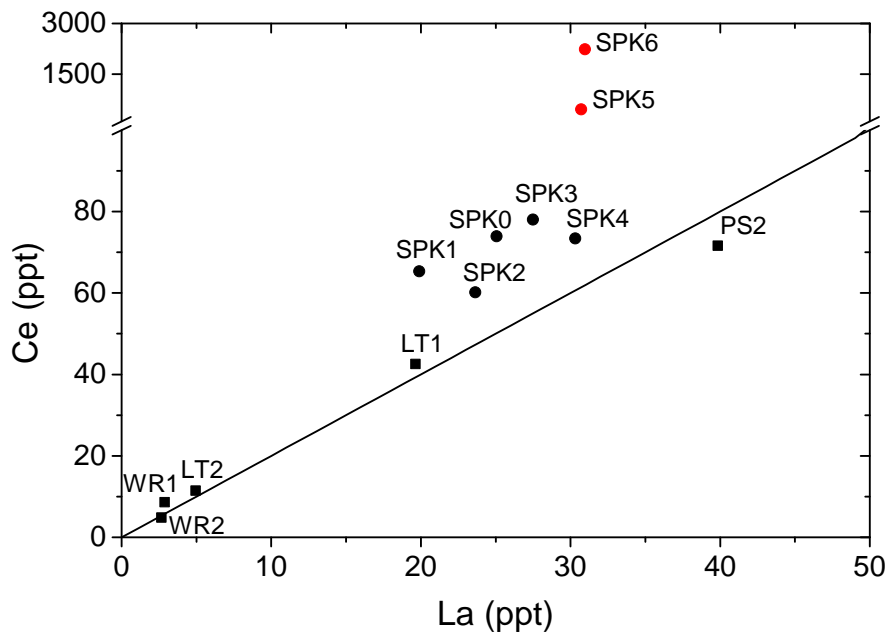


Figure 4.2: La and Ce particle mass concentrations detected by SP-ICP-MS. Square symbols and round symbols represent environmental samples and spiked samples, respectively. The highest spike concentrations have an increased Ce:La ratio and are plotted in red. The theoretical Ce:La ratio for uncontaminated samples of 2:1 is shown as the solid line in the graph.

CeO₂ NP test suspensions, not used in the spiking experiment, had a zeta potential of +20 mV, which might have lead to attachment, and therefore loss, to negatively charged surfaces. For the SRNOM stabilized spike suspensions 3–6 zeta potentials were determined between –89 and –91 mV, indicating the success of coating the CeO₂ NPs with negatively charged NOM. For spiking suspensions 1 and 2 no Zeta potential could be determined due to the low particle concentrations. The Z-average size was between 290 and 370 nm for suspensions 1–5, with suspension 6 showing bigger sizes with an average of 770 nm. In comparison with the manufacturer stated diameter of <50 nm, the Z-average sizes indicate homo-aggregation of the particles, which could not be reversed by bath sonication. Further characterization of the particle suspensions could be achieved by transmission electron microscopy to gain insights on the 3D shapes of the particle aggregates.

4.2.2 Ce recovery in spiked samples

Table 4.4 shows the amount of cerium spiked to the soils, the Ce concentrations of the <32µm fractions as well as the colloid fractions and the amount of spiked Ce recovered in those fractions. The natural Ce concentration of the bulk unspiked soil sample SPK0 was not determined, but approximated as 73 mg kg⁻¹, which is the Ce content of the respective <32µm fraction. Soil samples SPK3–SPK6 yielded 38–41% <32µm fractions, which hosted 64–73% of the Ce added (spiked Ce recovery). This shows that the CeO₂ NP powder enriched within the <32µm fraction of the soil. It must be noted that an even higher yield of the <32µm fractions could have been gained with a higher amount of water used for the wet-sieving process, and therefore a higher Ce recovery could have been accomplished. The amount of water used for wet-sieving was chosen as a compromise between sieving efficiency and time needed for the freeze drying of the wet sieved fractions.

For the low spike levels SPK0–SPK4 the Ce concentrations were lower in the colloid fraction than in the <32µm fractions, which is in agreement with the theory of selective loss of natural REE containing particles during centrifugation of the extracts. The higher spike levels SPK5 and SPK6 show an increase of the Ce concentration from the <32µm fraction to the colloid fraction, indicating an enrichment of spiked nCe, which might have sorbed onto minerals which were selectively enriched during the extraction process (e.g. clays). The nCe recoveries from soil to suspended colloidal matter (SCM) were between 20 and 23% for the high spiked concentrations SPK4–SPK6. Comparison of those nCe recoveries with the total SCM extraction yields of the respective samples of 13–14% (see Table 4.1) also shows that the

spiked nCe enriched within the colloidal fraction.

Further centrifugation of the extracts might remove even more natural high density Ce- and La-containing minerals and increase the relative amount of spiked CeO₂ adsorbed to clay particles. This would lead to a higher relative amount of nCe in the colloid extracts, causing a stronger shift in the Ce:La ratio (see below). If this holds true and nCe also adsorbs to clay particles in the environment, the aqueous extraction method would be an ideal sample preparation technique, amplifying the shift of the Ce:La ratio caused by presence of nCe.

Sample	Ce added to soil		Ce concentration		Spiked Ce recovery	
	(as CeO ₂) (% of Ce-BG)	(mg kg ⁻¹)	<32µm (mg kg ⁻¹)	SCM (mg kg ⁻¹)	<32µm (%)	SCM (%)
SPK0	0	0	73	55	bdl	bdl
SPK1	0.0045	0.0033	74	59	bdl	bdl
SPK2	0.045	0.033	72	53	bdl	bdl
SPK3	0.45	0.33	74	46	bdl	bdl
SPK4	4.5	3.3	79	59	73	20
SPK5	45	33	130	150	67	23
SPK6	450	330	610	1000	64	23

Table 4.4: Total Ce concentrations in the <32µm fractions and suspended colloidal matter (SCM) extracted from soils spiked with nCe determined by ICP-MS. Cerium concentrations and respective Ce-background (Ce-BG) equivalents added as CeO₂ to a soil with 73 mg kg⁻¹ Ce-background. Cerium recoveries state the amount of spiked nCe recovered in the fractions.

Bulk Ce:La ratios in spiked samples

The Ce:La ratios of the spiked samples are shown in Table 4.5. The ratios of the low spike levels SPK0–SPK4 in the <32µm fractions were between 2.0 and 2.1, with an average of 2.1 ± 0.1 , which is within the range of natural, uncontaminated soils. A significant shift in the ratio can be seen for samples SPK5 and SPK6 with 3.7 and 17.2, respectively. The Ce:La ratio for the colloid fractions of those samples is even higher with 6.6 and 40, respectively, which is due to the higher extraction efficiency of the spiked nCe compared to natural Ce and La containing particles. A shift of the Ce:La ratio in the colloid fraction could even be detected one concentration step below the <32µm detection limit, with SPK4 showing a Ce:La ratio of 2.5, which is significantly above the average ratio of SPK0–SPK3 with 2.05 ± 0.15 ($+3\sigma$). This shows that the addition of nCe of only 4.5% of the natural Ce-background concentration could be detected using the Ce:La ratio in a colloid suspension extracted

from soil. However, the Ce:La ratio of 2.5 in the colloid suspension of SPK4 is not significantly above the average of 2.05 ± 0.72 ($+3\sigma$) of all natural samples analyzed in this study (LT1, LT2, PS2 and SPK0). Because the amount of natural samples analyzed is low and measurements of LT2 were close to the detection limit, analysis of a broad selection of soil colloid extracts would be needed to evaluate the stability of the Ce:La ratio of colloidal extracts compared to their source material.

Sample	Ce:La ratios			
	expected	<32 μ m	colloids	colloids SP
SPK0	2.0	2.0	2.0	2.9
SPK1	2.0	2.0	2.1	3.3
SPK2	2.0	2.1	2.1	2.5
SPK3	2.0	2.1	2.0	2.8
SPK4	2.1	2.1	2.5	2.4
SPK5	3.0	3.7	6.6	15
SPK6	11	17	40	72

Table 4.5: Ce:La ratios of spiked soil samples analyzed by ICP-MS and SP-ICP-MS (colloids SP). The expected Ce:La ratios are based on the amount of nCe added to the soil with a known La and Ce background.

4.2.3 Single particle ICP-MS of spiked colloid samples

Single particle analysis was done in the same way as for the environmental samples described in section 4.1.4. Particle mass concentrations of colloid samples SPK0–SPK6 are shown in Figure 4.2 and the particle mass ratios of Ce:La are shown in Table 4.5. Ratios of Ce:La particle masses varied between 2.5 and 3.3 for the low concentrations SPK0–SPK4 which is higher than the ratios observed in the bulk colloid suspension (2.0–2.5). The increase of the Ce:La ratio from bulk colloid to single particle mass could either be from different dissolved concentrations of La and Ce in the suspensions, statistical errors of the data analysis or from inaccurate calibration curves. The determination of the dissolved La and Ce concentrations of colloid suspensions in future studies could help to solve this question.

For the highest spike concentrations SPK5 and SPK6 a particle mass Ce:La ratio of 15 and 72, respectively, was determined. Comparison with the respective bulk colloid Ce:La ratios of 6.6 and 40 show that the method used for single particle analysis might lower the limit of detection for technical CeO₂ NPs by showing a stronger shift of the Ce:La ratios. In contrast to this assumption the Ce:La ratio of SPK4 did not show a significant shift for the single particle mass analysis, which it

did for the bulk colloid analysis.

Apparent CeO₂ particle sizes were calculated for the Ce containing particle events detected by SP-ICP-MS. For the conversion of particle mass to size, a density of 7.65 cm⁻³ and a spherical shape were assumed. This is a simplification, as CeO₂ NPs can have various shapes including rods, cubes and spheres (Sun et al., 2012) and the shape of the particles used was not characterized. Also, when particle agglomerates are measured as "single particle events", the Ce measured is the total sum of the Ce-content of all particles, e.g. a CeO₂ ENP sorbed to a Ce-containing NNP. Neither does the simplified model include porosity of particle aggregates, meaning that the diameters determined were likely smaller than the actual diameter of the aggregates.

Size distribution histograms for samples SPK0 and SPK4–SPK6 are shown in Figure 4.3. Apparent CeO₂ diameters determined for SPK0 were in the range of 40–80 nm, with only very little particle events greater than 80 nm. This fits the assumption that relatively big metal oxide nanoparticles were removed during centrifugation because of their high density. Spiked samples SPK1–SPK3 showed a similar size distribution as the blank SPK0 (data not shown). Samples SPK0–SPK3 do not show single particle events above the size of 110 nm, but for SPK4 two events in the range of 110–150 nm could be detected. However, those particles could also be "double events", meaning that two or more particles were combusted in the ICP-MS simultaneously and interpreted as a single particle (Laborda et al., 2013). For a relatively "safe" detection of big particles, longer sample measurement times combined with further dilutions would reduce the probability of double events. The amount of particles >100 nm increases noticeably in SPK5, showing a homogeneous distribution from 90–160 nm. Spiked sample SPK6 shows an even broader size distribution, with a relative increase of the 90–160 nm population. An increase of particles detected in the size range of 40–60 nm could also be detected for samples SPK5 and SPK6, which can not be seen in the histograms showing a relative frequency distribution.

Centrifugation during the extraction process produced a cut-off of 150 nm for spherical particles with a density of 7.65 g cm⁻³ (equation 3.1), which fits the low detected number of CeO₂ particles >150 nm. However, real aggregate sizes (e.g., CeO₂ adsorbed to clay particles) can not be determined using SP-ICP-MS theory, unless combined with another size separation technique, such as A4F.

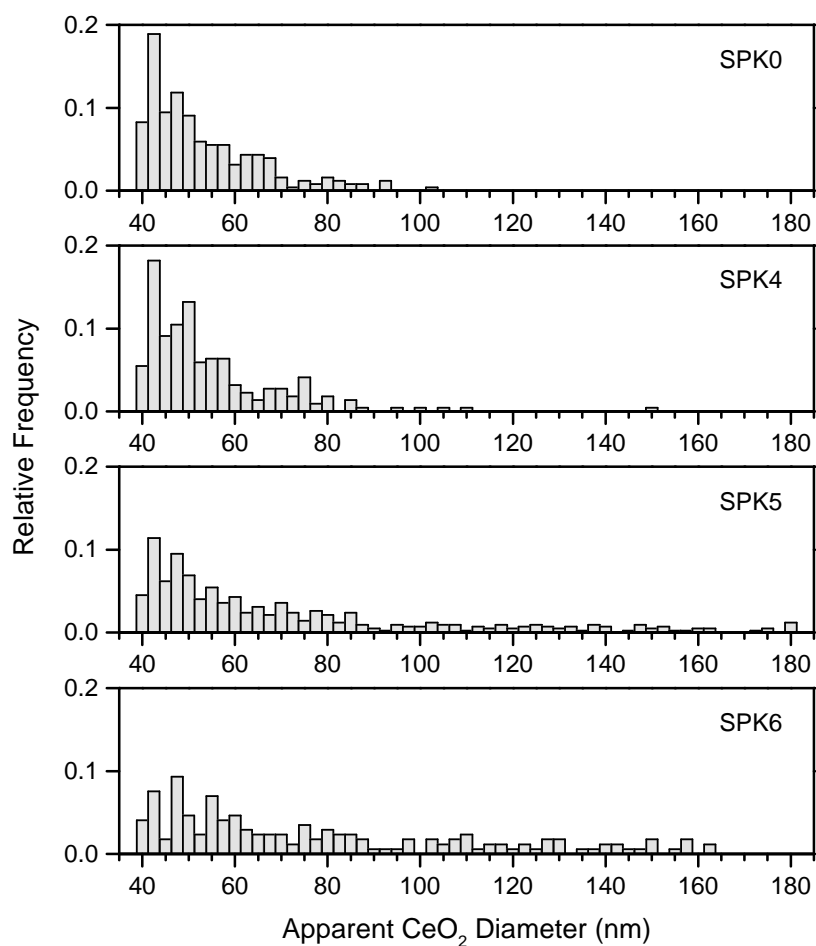


Figure 4.3: Apparent CeO₂ particle size histograms from single particle ICP-MS data. Samples SPK4, SPK5 and SPK6 were spiked with increasing amounts of CeO₂ NPs, SPK0 is a blank.

4.2.4 A4F-ICP-MS coupling of spiked colloid samples

A4F method optimization

The aim of A4F is a continuous size separation of a sample with a high resolution and a minimum of sample loss during the process. For the samples analyzed by A4F-ICP-MS coupling, an ammonium carbonate solution was chosen as the carrier liquid because preliminary A4F test runs of colloid extracts had shown good separation behaviour combined with a good recovery. The first step in method development was the optimization of the most sensible parameter, the cross flow. Multiple cross flow rates between 0.35 and 1.2 mL min⁻¹ were tested. Low cross flows showed poor resolution, with the sample peak not being properly separated from the void peak, whereas high cross flows showed a good resolution but poor sample recoveries as little as 40%. A cross flow of 0.6 mL min⁻¹ showed to be a compromise between separation resolution and sample loss from attachment to the channel. After setting a fixed cross flow, different ammonium carbonate concentrations were tested. Changing the ionic strength (IS) in the carrier liquid has the main effect of compressing the electric double layer around particles with a high charge, and therefore reducing the distance of those particles to the membrane. FFF theory does not involve electrostatic interactions between the particles and membrane, so limiting those effects is favourable. However if the ionic strength is too high, attachment of particles to the membrane can happen, resulting in a selective loss of big particles. Other partly unwanted effects of carrier additives are the formation of particle aggregates or changes in the surface chemistry of the particles, causing a change of their hydrodynamic radius. In this study ammonium carbonate concentrations of 0.09, 0.15, 0.20, and 0.30 mM were tested, resulting in recoveries of 100, 91, 87 and 82%. A concentration of 0.15 mM was chosen for the final method because of its good recovery of 91 % and a good elution behaviour of the sample.

MALLS and radius of gyration

Size separation using an A4F system prior to mass analysis in an ICP-MS was done for 50 µL of the diluted (1:20) colloid suspensions SPK0 and SPK3–SPK6. Light scattering data was collected using a MALLS device. Signals of sample SPK0 for the detectors at 32° and 90° as well as the calculated radius of gyration values (r_g) are shown in Figure 4.4 A). Elution volume was converted into a hydrodynamic diameter (D_h) using an alternative calibration (section 3.6.3). Sizes mentioned from now on will refer to the calibrated D_h , unless otherwise stated.

All spiked samples showed a similar elution behaviour and light scattering, there-

fore only SPK0 will be discussed as an example. Particles causing a noticeable light scattering signal started eluting at 60 nm with a respective r_g of 30 nm. The peak maximum for the 90° and 32° detectors are at 290 and 320 nm, respectively. The maximum of the 32° detectors are later in the elution because of the fact that large particles show more scattering at low angles, whereas small particles scatter light more homogeneously into all angles (v. d. Kammer et al., 2005). This can also be seen at the end of the peak, where the 90° signal reaches the baseline before the 32° signal. On the high diameter side of the 32° signal there is a shoulder, indicating the presence of particles too large for the chosen channel dimensions. This can also be seen in a rise of the slope of r_g at 400 nm. The ratio of $r_g:D_h$ is in the range of $\sim 2:1$ from the beginning of the peak to 220 nm (D_h). Beginning at 220 nm (D_h), the slope of the r_g inclines, resulting in higher ratios of $r_g:D_h$. As the r_g is calculated by the mass distribution within one particle, differently shaped particles with the same r_g could have different D_h sizes. The ratio of $r_g:D_h$ can be used to describe the shape of a particle, with higher ratios indicating non spherical particles, e.g. rods or platelets (v. d. Kammer et al. (2005), Plathe et al. (2010)). However, this approach can only be used accurately for the description of relatively monodisperse samples. The A4F system used for the analysis in this study showed to have focussing problems after the experiments were conducted, which might have also had an influence on the runs of this study. However, overall elution behaviour was considered to be acceptable, and similar to an aqueous colloid extract gained with a similar method Plathe et al. (2010). The average recovery (90° MALLS signal) for all samples was $100 \pm 2.2\%$, showing no loss of sample to the membrane.

Al and Fe fractionation

The mass signals for Al and Fe show a completely different shape than the MALLS signals (Figure 4.4 B). The maximum of the light scattering signal around 300 nm can be seen in the Al and Fe signals, but another peak, eluting earlier at 140 nm, is clearly visible for both, Al and Fe. Producing no MALLS response, the mass being detected in the ICP-MS could have either been:

- Dissolved Al and Fe
- Dissolved organic matter
- Matter with a refractive index identical to that of the carrier
- Small particles

Dissolved Al and Fe would have been removed during the focusing step in the A4F and dissolved organic matter is typically smaller <30 nm and would therefore elute very close to the void peak. Matter with a refractive index close to that of water does exist, but has not been found in high concentrations in natural colloid suspensions. Therefore the peak at 140 nm is probably from very small particles which scatter light below the detection limit of the MALLS, as the scattering intensity increases with r^3 (radius of the particle) for constant particle mass concentrations (v. d. Kammer, 2004).

Both Al and Fe have a very similar mass distributions, which might be because both elements are mainly incorporated into clay minerals. Only in the size range from 20 to 100 nm there is a noticeable difference, with Fe being present at higher concentrations than Al, which might show the presence of small Fe-oxides. Larger Fe-oxides (>150 nm), even if extracted from the soil, would have been removed during the centrifugation step of the extraction, which fits to the peak in the 20 to 100 nm (Dh) range. Recoveries determined by recovery runs were 103 ± 0.9 and 103 ± 0.7 for Al and Fe, respectively, showing no loss of Al and Fe containing particles.

La and Ce fractionation

The Ce and La mass fractograms and the Ce:La ratio for the spike blank SPK0 are shown in Figure 4.4 C). Both elements show a similar distribution, having only one maximum around 220 nm. Thin lines represent the raw instrument signal, which is noisy because of the short integration time of 0.2 s. Finding a suitable smoothing algorithm proved to be difficult, because of the high noise and single high concentration events in the spiked samples. A simple Adjacent-Averaging algorithm (130 points, weighted average) seemed to be a good solution because it does not remove high concentration events, which should still be noticeable in the smoothed signal. At 20 nm Ce has a distinct peak maximum, which can not be seen in the La signal. This might show the presence of a mineral phase containing significantly more Ce than La. Cerium can occur as Ce^{3+} and Ce^{4+} , with the Ce^{4+} ion having a smaller radius than the four-valent form. Lanthanum on the other hand can only occur as La^{2+} and La^{3+} . Because Ce^{4+} has the same charge and a similar ionic radius as Zr^{4+} ($\text{Ce}^{4+} = 0.97$; $\text{Zr}^{4+} = 0.84 \text{ \AA}$), it can replace the Zr^{4+} ion in minerals such as zirconium (Thomas et al., 2003). Lanthanum can only have oxidation states of 2+ and 3+, and is therefore not favourable for substitution of four-valent ions. This can cause a positive Ce anomaly, which could be the cause the distinct Ce signal in SPK0 in the size range of 20–60 nm, where the Ce:La is in the range of 2.5–3.5. With only the

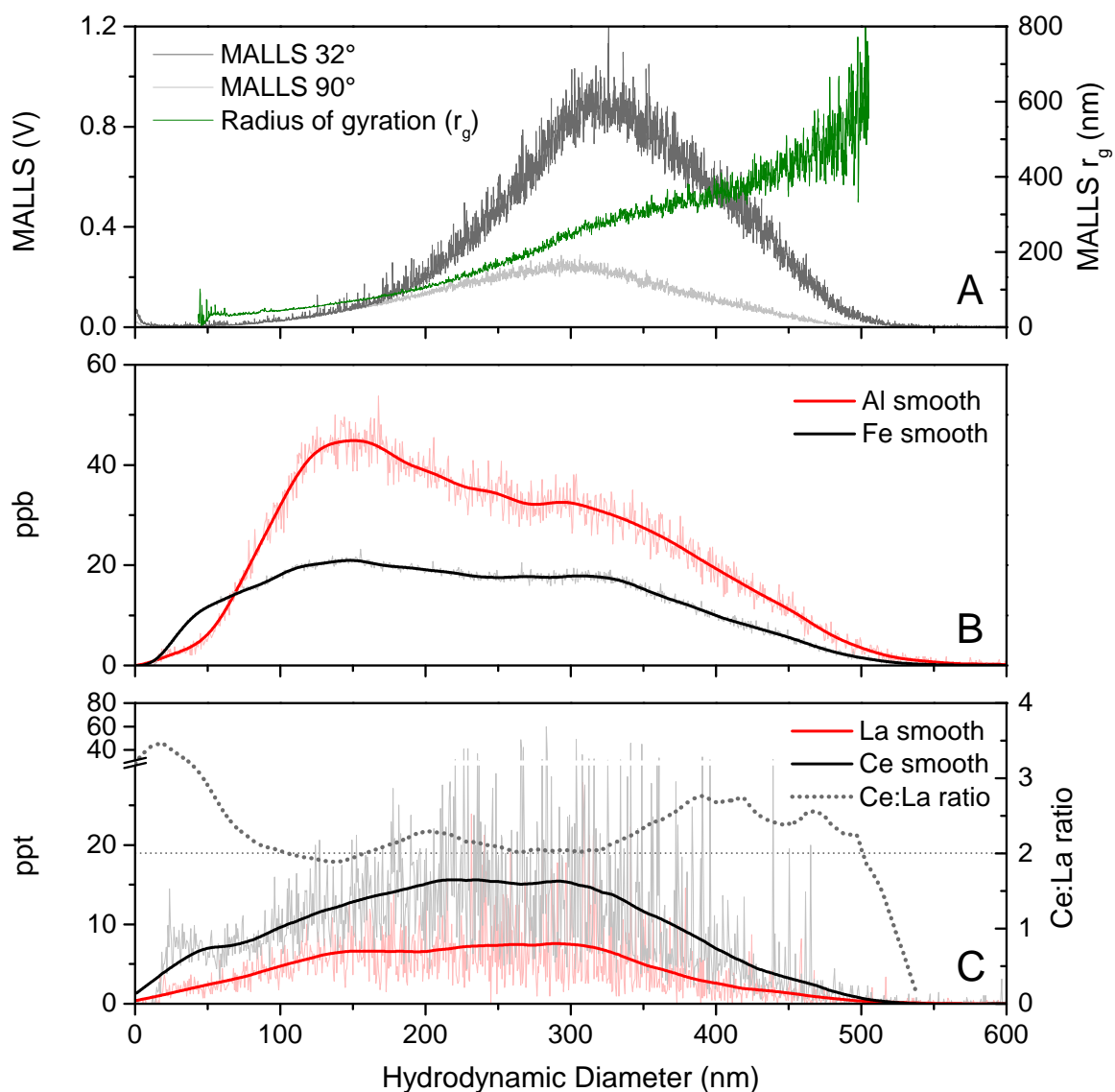


Figure 4.4: A4F-ICP-MS coupling of colloidal sample SPK0, elution volume has been converted to hydrodynamic diameter. A) MALLS signal for detectors 32°/90° and calculated radius of gyration. B) Al and Fe mass signals C) La and Ce mass signals and Ce:La ratio. In panels B) and C) thin lines represent the raw signal.

A4F-ICP-MS data it is not possible to determine which mineral phase shows the positive Ce anomaly in SPK0, however collection of the size fraction and analysis by another method such as EDX could identify the mineral phase. A slight increase of the Ce:La ratio in blank SPK0 can also be seen in the size range of 350–500 nm, which is due to a small amount of sharp peaks, likely caused by single particle events. Except for those two maxima, the Ce:La ratio is stable and close to 2:1.

Figure 4.5 shows the La and Ce mass fractograms of the spiked Samples SPK3–SPK6 as well as SPK0 for comparison. All samples were analyzed within one day and without a change of the A4F membrane and in the order of increasing CeO₂ spike concentrations, except for SPK3, which was measured after the highest concentration, SPK6. All samples, independent of the CeO₂ concentration added, show the positive Ce anomaly in the size range of 20–60 nm. Sample SPK3 shows a similar Ce:La ratio as SPK0, except for a maximum of 4.2 in the size range of 500 nm due to the presence of two high concentration events. Although the channel was flushed for 10 min before SPK3 was analyzed, it is possible that some CeO₂ particles of the previous runs could have carried over. Even when excluding the big Ce-containing events in SPK4, an increase of the Ce:La ratio with the hydrodynamic diameter can be seen. This trend gets stronger in SPK5 and SPK6, indicating that the spiked CeO₂ NPs either form homo-aggregates with a hydrodynamic diameter in the size range of 150–500 nm, or adsorb to particles of that size class. As sizes determined by SP-ICP-MS of spiked samples SPK5 and SPK6 show a maximum in the size range of 40–60 nm it is more likely that the spiked CeO₂ form hetero-aggregates with natural colloid particles.

The coupling of A4F-ICP-MS could not lower the detection limit for spiked CeO₂ NPs directly, but supplied some information about the behaviour of the spiked CeO₂ NPs. Collection of the fraction from 200 to 400 nm, which had the highest spiked CeO₂ concentration, and analysis via SP-ICP-MS might lower the detection limit for nCe in colloid suspensions extracted from soils. If the CeO₂ particles formed hetero-aggregates with clay particles, it would also be possible to enrich the spiked Ce content in the colloid extracts by further centrifugation. Although promising, those theories were not tested and might be subject for further studies.

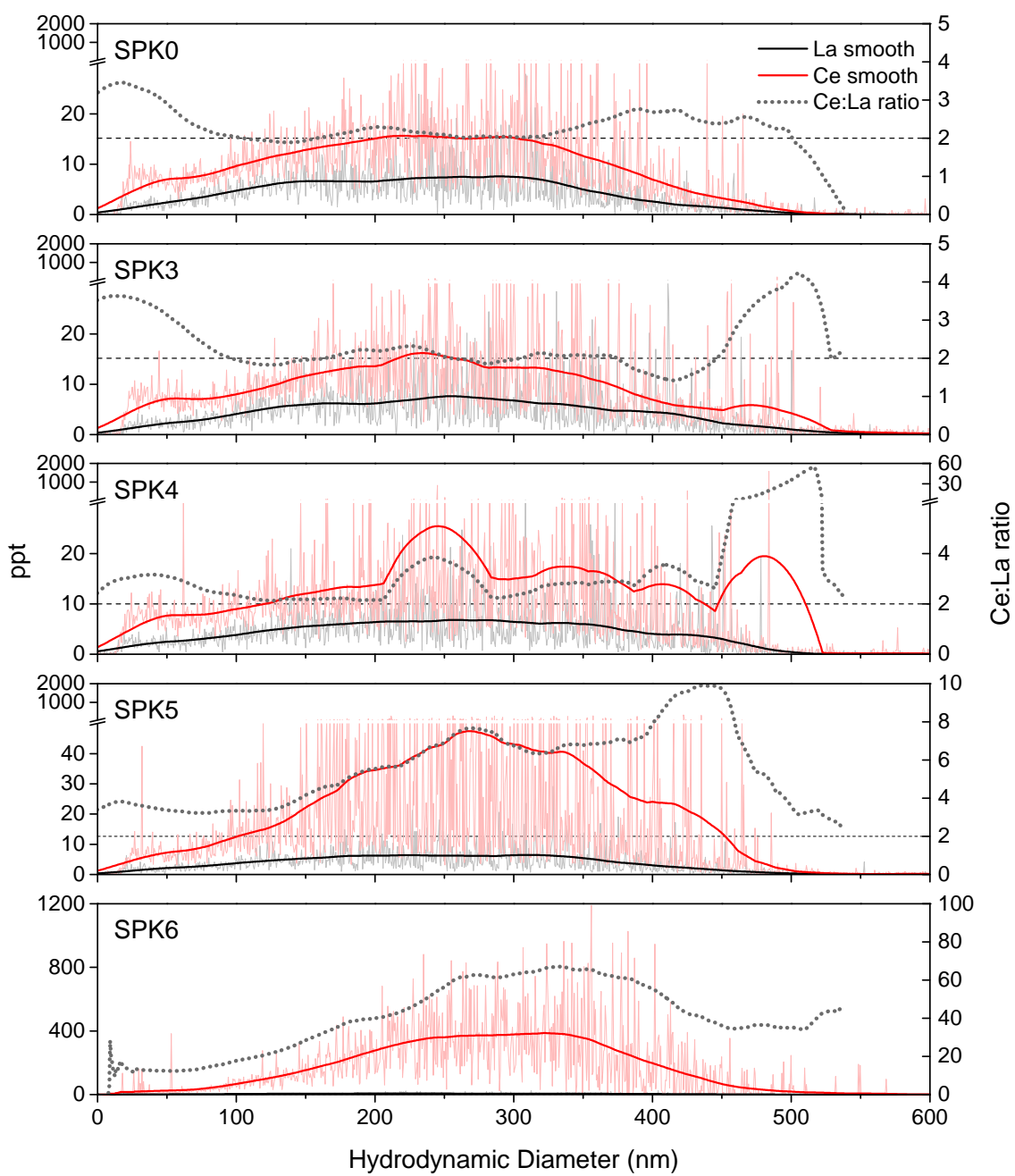


Figure 4.5: A4F-ICP-MS data for La and Ce of spiked colloidal samples with different Ce concentrations added.

5 Conclusions and Outlook

This work demonstrates the use of the Ce:La ratio for detection of technical CeO₂ nanoparticles in soil fractions <32µm and colloid suspensions extracted from soil. Natural samples analyzed showed a Ce:La ratio of 2.0:1 (±0.1) and 2.0:1 (±0.2) for the <32µm soil fraction and extracted colloids, respectively. Those ratios are in agreement with ratios for soils and sediments reported by v. d. Kammer et al. (2013) and suggest that shifts of the ratio might be used for detection of engineered CeO₂ NPs. Because only four natural samples were studied in this work, future analysis of a broad selection of soil colloid extracts would be needed to evaluate the stability of the Ce:La ratio in the colloid fractions.

A spiking experiment was conducted to determine the detection limits for nCe added to a soil by the use of the Ce:La ratio. Using the Ce:La ratio, the addition of nCe to a soil at a concentration of 4.5% of the natural background could be detected by bulk mass analysis of a colloid suspension extracted from that soil (3.3 ppm Ce added to 73 ppm soil background). The highest Ce:La ratio, indicating the most sensitive technique, of 72:1 was observed via single particle analysis, compared to 40:1 determined via bulk analysis of the same spiked sample. However, the addition of nCe equalling 4.5% of the natural background could not be detected via SP-ICP-MS, but could be detected using the bulk Ce:La ratio. This shows that SP-ICP-MS is a promising technique which needs further attention, especially in the method development. Size separation of the spiked colloidal samples by A4F and coupling to an ICP-MS has shown that the spiked CeO₂ NPs were enriched in the size range of 200–400 nm (hydrodynamic diameter). An increase of the Ce:La ratio in the A4F-ICP-MS mass fractograms could be detected at an added nCe concentration of 4.5% of the natural background, which is the same detection limit as for the bulk colloid analysis. Collection of the relatively CeO₂ enriched A4F-fraction and further bulk- or single particle analysis via ICP-MS might be able to push the detection limit for nCe even lower.

Future studies including possibly contaminated soil samples from areas where nCe is used as a diesel fuel additive could show the real world applicability of the Ce:La ratio for detection of nCe in the environment. Another cause for higher ra-

tios of Ce:La in uncontaminated environmental matrices could be natural positive cerium anomalies (Andersson et al. (2006), Thomas et al. (2003)), showing the need for further research to evaluate the commonness of positive Ce anomalies in different matrices.

Another promising technique for the detection of nCe not used in this study is Inductively Coupled Plasma Time-of-Flight Mass Spectrometry (v. d. Kammer et al., 2015), which enables the simultaneous detection of multiple elements within one single particle. The simple idea behind the detection of nCe using this technique is that particles showing a Ce signal but no La signal are most probably technical CeO₂ nanoparticles, making it easy to directly count those particles without the statistical and theoretical detour of using the Ce:La ratio. Although very promising, the technique is still under early development with current size detection limits for CeO₂ in the range of 60–100 nm (v. d. Kammer et al., 2015).

The only CeO₂ nanoparticle consumer products currently available are various diesel fuel additives (Edward and Spiros (2010)), limiting the possibilities for release scenarios into the environment. Because of its unique properties, new applications for CeO₂ NPs will likely be found in the future, opening up new ways of environmental release scenarios for a material of which the environmental impact and toxicity are not well understood (Collin et al. (2014), Gambardella et al. (2014)). This study proposes a sensitive tool for the detection of CeO₂ nanoparticles, which might be especially useful in the case that nanoparticulate CeO₂ shows to cause adverse health effects on humans or other species.

6 Bibliography

- Andersson, K., Dahlgvist, R., Turner, D., Stolpe, B., Larsson, T., Ingri, J., and Andersson, P. (2006). Colloidal rare earth elements in a boreal river: Changing sources and distributions during the spring flood. *Geochimica et Cosmochimica Acta*, 70(13):3261 – 3274.
- Atademir, M., Kitchener, J., and Shergold, H. (1979). The surface chemistry and flotation of scheelite: Solubility and surface characteristics of precipitated calcium tungstate. *Journal of Colloid and Interface Science*, 71(3):466 – 476.
- Baalousha, M., v. d. Kammer, F., Motelica-Heino, M., Hilal, H., and Coustumer, P. L. (2006). Size fractionation and characterization of natural colloids by flow-field flow fractionation coupled to multi-angle laser light scattering. *Journal of Chromatography*, 1104(1–2):272 – 281.
- Beckett, R. and Hart, B. (1993). Use of field-flow fractionation techniques to characterize aquatic particles, colloids, and macromolecules. *Environmental Particles*, 2:165–205.
- Bernhardt, C. (1994). *Particle size analysis: Classification and sedimentation methods*. Chapman & Hall, London.
- Carpenter, M. A., Mathur, S., and Kolmakov, A., editors (2012). *Metal Oxide Nanomaterials for Chemical Sensors*. Springer.
- Cassee, F. R., van Balen, E. C., Singh, C., Green, D., Muijser, H., Weinstein, J., and Dreher, K. (2011). Exposure, health and ecological effects review of engineered nanoscale cerium and cerium oxide associated with its use as a fuel additive. *Crit. Rev. Toxicol.*, 41(3):213–229.
- Collin, B., Oostveen, E., Tsyusko, O. V., and Unrine, J. M. (2014). Influence of natural organic matter and surface charge on the toxicity and bioaccumulation of functionalized ceria nanoparticles in caenorhabditis elegans. *Environmental Science & Technology*, 48(2):1280–1289. PMID: 24372151.

- Councell, T. B., Duckenfield, K. U., Landa, E. R., and Callender, E. (2004). Tire-wear particles as a source of zinc to the environment. *Environmental Science & Technology*, 38(15):4206–4214. PMID: 15352462.
- Degueldre, C. and Favarger, P.-Y. (2003). Colloid analysis by single particle inductively coupled plasma-mass spectroscopy: a feasibility study. *Colloids and Surfaces A: Physicochemical and Engineering Aspects*, 217(1–3):137 – 142. Symposium C of the E-MRS 2002 Spring Meeting in Strasbourg, France.
- Edward, M. H. and Spiros, A. P. (2010). Characterizing concentrations and size distributions of metal-containing nanoparticles in waste water. Epa/600/r-10/117, U.S. Environmental Protection Agency, Washington, DC.
- EPA, U. S. (2007). Nanotechnology white paper. Epa/100/b-07, U.S. Environmental Protection Agency, Washington, DC. <http://www.epa.gov/osa/pdfs/nanotech/epa-nanotechnology-whitepaper-0207.pdf>.
- Gambardella, C., Mesarič, T., Milivojević, T., Sepčić, K., Gallus, L., Carbone, S., Ferrando, S., and Faimali, M. (2014). Effects of selected metal oxide nanoparticles on artemia salina larvae: evaluation of mortality and behavioural and biochemical responses. *Environmental Monitoring and Assessment*, 186(7):4249–4259.
- Gantt, B., Hoque, S., Willis, R. D., Fahey, K. M., Delgado-Saborit, J. M., Harrison, R. M., Erdakos, G. B., Bhav, P. V., Zhang, K. M., Kovalcik, K., and Pye, H. O. T. (2014). Near-road modeling and measurement of cerium-containing particles generated by nanoparticle diesel fuel additive use. *Environmental Science Technology*, 48:10607–10613.
- Gondikas, A., v. d. Kammer, F., Reed, R., Wagner, S., Ranville, J., and Hofmann, T. (2014). Release of tio2 nanoparticles from sunscreens into surface waters: A one-year survey at the old danube recreational lake. *Environmental Science & Technology*, 48:5415–5422.
- Jennings, B. R. and Parslow, K. (1988). Particle size measurement: The equivalent spherical diameter. *Proceedings of the Royal Society of London A: Mathematical, Physical and Engineering Sciences*, 419(1856):137–149.
- Karjalainen, P., Pirjola, L., Heikkilä, J., Lähde, T., Tzamkiozis, T., Ntziachristos, L., Keskinen, J., and Rönkkö, T. (2014). Exhaust particles of modern gasoline vehi-

- cles: A laboratory and an on-road study. *Atmospheric Environment*, 97(0):262 – 270.
- Kim, H.-A., Choi, Y. J., Kim, K.-W., Lee, B.-T., and Ranville, J. F. (2012). Nanoparticles in the environment: stability and toxicity. *Rev Environ Health*, 27(4):175–179.
- Laborda, F., Jimenez-Lamana, J., Bolea, E., and Castillo, J. R. (2013). Critical considerations for the determination of nanoparticle number concentrations, size and number size distributions by single particle icp-ms. *J. Anal. At. Spectrom.*, 28:1220–1232.
- Meisterjahn, B., Neubauer, E., der Kammer, F. V., Hennecke, D., and Hofmann, T. (2014). Asymmetrical flow-field-flow fractionation coupled with inductively coupled plasma mass spectrometry for the analysis of gold nanoparticles in the presence of natural nanoparticles. *Journal of Chromatography A*, 1372(0):204 – 211.
- Neubauer, E., v.d. Kammer, F., and Hofmann, T. (2013). Using flowfff and hpsec to determine trace metal-colloid associations in wetland runoff. *Water Research*, 47(8):2757 – 2769.
- Nowicki, W. and Nowicka, G. (1994). Verification of the schulze-hardy rule: A colloid chemistry experiment. *Journal of Chemical Education*, 71(7):624.
- O'Brien, N. and Cummins, E. (2008). Recent developments in nanotechnology and risk assessment strategies for addressing public and environmental health concerns. *Human and Ecological Risk Assessment: An International Journal*, 14(3):568–592.
- Och, L. M., Müller, B., Wichser, A., Ulrich, A., Vologina, E. G., and Sturm, M. (2014). Rare earth elements in the sediments of lake baikal. *Chemical Geology*, 376(0):61 – 75.
- Ohta, A. and Kawabe, I. (2000). Rare earth element partitioning between Fe oxyhydroxide precipitates and aqueous NaCl solutions doped with NaHCO₃: Determinations of rare earth element complexation constants with carbonate ions. *Geochemical Journal*, 34:439–454.
- Pace, H. E., Rogers, N. J., Jarolimek, C., Coleman, V. A., Higgins, C. P., and Ranville, J. F. (2011). Determining transport efficiency for the purpose of counting and sizing nanoparticles via single particle inductively coupled plasma mass spectrometry. *Analytical Chemistry*, 83(24):9361–9369.

- Plathe, K. L. (2010). *Nanoparticle - Heavy Metal Associations in River Sediments*. PhD thesis, Virginia Polytechnic Institute and State University.
- Plathe, K. L., von der Kammer, F., Hassellöv, M., Moore, J., Murayama, M., Hofmann, T., and Hochella, M. F. (2010). Using FIFFF and aTEM to determine trace metal-nanoparticle associations in riverbed sediment. *Environ. Chem.*, 7:82–93.
- Plathe, K. L., von der Kammer, F., Hassellöv, M., Moore, J. N., Murayama, M., Hofmann, T., and Jr., M. F. H. (2013). The role of nanominerals and mineral nanoparticles in the transport of toxic trace metals: Field-flow fractionation and analytical TEM analyses after nanoparticle isolation and density separation. *Geochimica et Cosmochimica Acta*, 102(0):213 – 225.
- Sun, C., Li, H., and Chen, L. (2012). Nanostructured ceria-based materials: synthesis, properties, and applications. *Energy Environ. Sci.*, 5:8475–8505.
- Thomas, J. B., Bodnar, R. J., Shimizu, N., and Chesner, C. A. (2003). Melt inclusions in zircon. *Reviews in Mineralogy and Geochemistry*, 53:63–87.
- v. d. Kammer, F. (2004). *Characterization of Environmental Colloids applying Field-Flow Fractionation - Multi Detection Analysis with Emphasis on Light Scattering Techniques*. PhD thesis, Technische Universität Hamburg-Harburg.
- v. d. Kammer, F., Baborowski, M., and Friese, K. (2005). Field-flow fractionation coupled to multi-angle laser light scattering detectors: Applicability and analytical benefits for the analysis of environmental colloids. *Analytica Chimica Acta*, 552(1–2):166 – 174.
- v. d. Kammer, F., Ferguson, P. L., Holden, P. A., Masion, A., Rogers, K. R., Klaine, S. J., Koelmans, A. A., Horne, N., and Unrine, J. M. (2012). Analysis of engineered nanomaterials in complex matrices (environment and biota): General considerations and conceptual case studies. *Environmental Toxicology and Chemistry*, 31(1):32–49.
- v. d. Kammer, F. and Neubauer, E. (2013). Detectnano preliminary report. Technical report, University of Vienna, Department of Environmental Geosciences.
- v. d. Kammer, F., Neubauer, E., Reed, R. B., Ranville, J. F., and Hofmann, T. (2013). Detection of engineered cerium oxide nanoparticles in the environment. In *Goldschmidt Conference 2013*.

- v. d. Kammer, F., Praetorius, A., Fabienke, W., Wagner, S., Graham-Gundlach, A., Borovinskaya, O., L., H., Navratilova, J., Velimirovic, M., Neubauer, E., Günther, D., and Hofmann, T. (2015). Detection of engineered cerium oxide nanoparticles in soil extracts. In *European Winter Conference on Plasma Spectrochemistry 2015*.
- Zagaynov, I. and Kutsev, S. (2014). Formation of mesoporous nanocrystalline ceria from cerium nitrate, acetate or acetylacetonate. *Applied Nanoscience*, 4(3):339–345.
- Zdzisław, M. M. and Agnieszka, G. (2015). The characteristics, occurrence, and geochemical behavior of rare earth elements in the environment: A review. *Critical Reviews in Environmental Science and Technology*, 45(5):429–471.

7 Appendix

7.1 Abbreviations

A4F	Asymmetric Flow Field-flow fractionation
BG	background
CPS	counts per second
DL	detection limit
DF	detector flow rate
ENP	engineered nanoparticle
ETA	estimated transport efficiency
FFF	Field-flow fractionation
ICP-MS	inductively coupled plasma mass spectrometry
ICP-OES	inductively coupled plasma optical emission spectrometry
IS	ionic strength
LC	long channel
MALLS	multi-angle laser light scattering
NOM	natural organic matter
NNP	natural nanoparticle
PMP	polymethylpentene
r_g	radius of gyration
REE	rare earth elements
rpm	revolutions per minute
rec	recovery
SCM	suspended colloidal matter
SP-ICP-MS	Single particle inductively coupled plasma mass spectrometry
SRNOM	Suwannee River Natural Organic Matter
TOC	total organic carbon
TRA	time resolved analysis (single particle mode)
XF	cross flow

7.2 Additional Tables and Figures

Sample	number concentration			mass concentration			CeO ₂ \varnothing
	Ce ($\times 10^7$ mL ⁻¹)	La	Ce:La ratio	Ce (ng mL ⁻¹)	La (ng mL ⁻¹)	Ce:La ratio	(nm)
LT1	7.8	6.7	1.2	43	20	2.2	53 \pm 12
LT2	1.3	1.4	0.98	11	5.0	2.3	58 \pm 18
WR1	1.4	1.1	1.3	8.6	2.9	3.0	53 \pm 14
WR2	0.59	0.56	1.1	4.8	2.7	1.8	57 \pm 18
PS2	14	15	0.96	72	40	1.8	51 \pm 11
SPK0	13	9.0	1.4	74	25	2.9	53 \pm 12
SPK1	11	8.6	1.3	65	20	3.3	54 \pm 11
SPK2	11	8.3	1.3	60	24	2.5	53 \pm 11
SPK3	13	11	1.2	78	27	2.8	54 \pm 13
SPK4	11	12	0.93	73	30	2.4	54 \pm 15
SPK5	21	12	1.8	450	31	15	71 \pm 33
SPK6	87	11	8.0	2200	31	72	78 \pm 34

Table 7.1: Single particle data for Ce and La for selected samples. The CeO₂ diameter is calculated as the average apparant particle diameter assuming spherical geometry.

Sample	LOI (%)	Be (ppm)	Na (ppm)	Mg (ppm)	Al (ppm)	Si (ppm)	P (ppm)	K (ppm)	Ca (ppm)	Sc (ppm)	Ti (ppm)	Mn (ppm)	Fe (ppm)	V (ppm)	Cr (ppm)	Co (ppm)
PT1	22.3	2.52	6650	32400	61500	190000	762	17200	77600	12.7	3340	834	33800	96.0	71.0	14.7
PT2	33.2	2.00	6310	28100	53600	164000	809	15200	70200	13.5	2810	681	29900	89.0	60.0	13.7
PT3	23.5	3.02	5480	30500	65100	175000	756	18500	77300	19.9	3160	851	36400	108	72.8	15.1
PS1	15.6	2.52	4410	7870	75800	264000	586	17000	10900	13.5	4160	1230	40100	119	73.7	15.7
PS2	16.7	2.69	2350	8900	86700	250000	611	20200	13100	14.1	3970	668	38500	149	94.8	14.2
PS3	11.7	2.12	4710	7430	75000	285000	411	16300	5100	16.8	5050	499	35200	115	81.5	10.5
LT1	14.6	ND	3410	6240	66700	276000	523	14300	8270	15.5	4240	457	27900	110	87.0	6.70
LT2	13.4	ND	9780	7170	72800	279000	563	19900	1600	9.90	6690	272	24600	96.0	83.0	6.20
WR1	32.3	ND	4820	30200	43100	147000	1160	10700	79400	8.60	3240	2120	53600	126	260	15.1
WR2	32.6	ND	4790	34600	39100	123000	1110	9530	97000	9.10	3190	2490	53700	139	269	14.1
Sample	Ni (ppm)	Cu (ppm)	Zn (ppm)	As (ppm)	Rb (ppm)	Sr (ppm)	Zr (ppm)	Nb (ppm)	Mo (ppm)	Cd (ppm)	Sn (ppm)	Sb (ppm)	Cs (ppm)	Ba (ppm)	Tl (ppm)	Pb (ppm)
PT1	44.6	38.6	112	21.7	128	160	110	22.6	1.26	0.280	5.28	2.28	8.17	340	0.650	45.9
PT2	43.7	79.6	178	24.6	109	149	50.0	17.1	1.02	0.430	6.26	2.77	4.85	324	0.680	61.0
PT3	51.6	43.1	191	16.2	125	166	288	50.8	1.57	0.380	5.36	2.77	8.04	350	0.680	48.8
PS1	58.7	56.6	172	10.0	122	117	80.0	21.2	2.21	0.810	5.58	1.59	7.44	346	0.740	65.3
PS2	53.3	52.7	167	11.8	163	128	86.8	23.7	1.15	0.640	7.69	1.41	10.2	271	0.810	53.4
PS3	41.2	50.1	135	15.4	124	108	127	36.4	1.46	<0.1	5.11	1.83	6.94	301	0.620	35.5
LT1	ND	ND	ND	ND	86.0	116	176	71.1	ND	ND	ND	ND	8.70	250	0.680	41.0
LT2	ND	ND	ND	ND	85.0	68.0	111	27.5	ND	ND	ND	ND	3.80	484	0.820	70.0
WR1	ND	ND	ND	ND	49.0	112	101	20.4	ND	ND	ND	ND	5.30	490	0.670	117
WR2	ND	ND	ND	ND	42.0	130	92.0	20.6	ND	ND	ND	ND	5.10	445	0.620	102
Sample	Y (ppm)	La (ppm)	Ce (ppm)	Pr (ppm)	Nd (ppm)	Sm (ppm)	Eu (ppm)	Gd (ppm)	Tb (ppm)	Dy (ppm)	Ho (ppm)	Er (ppm)	Tm (ppm)	Yb (ppm)	Lu (ppm)	Th (ppm)
PT1	16.0	29.4	59.1	5.93	24.6	5.57	1.14	4.59	0.57	2.89	0.53	1.63	0.28	1.38	0.24	9.43
PT2	14.0	25.1	49.3	5.62	21.4	3.96	0.810	3.40	0.47	2.68	0.51	1.53	0.21	1.40	0.17	7.62
PT3	14.9	24.6	53.4	6.81	27.2	4.77	0.810	3.32	0.51	3.49	0.55	1.70	0.21	1.40	0.17	11.9
PS1	20.0	32.3	68.2	7.17	29.1	5.43	1.05	4.73	0.66	3.49	0.70	2.13	0.31	1.94	0.23	10.5
PS2	19.0	32.6	66.5	6.75	23.8	3.76	1.20	4.23	0.51	3.16	0.68	2.35	0.38	1.79	0.21	11.0
PS3	19.1	35.1	72.6	7.86	30.0	6.49	0.960	4.57	0.62	3.62	0.83	2.41	0.37	2.25	0.37	11.6
LT1	17.8	29.6	56.0	6.90	25.0	4.90	0.700	3.80	0.38	3.40	0.65	1.60	0.23	1.90	0.23	12.7
LT2	12.5	39.3	79.0	9.20	33.0	5.10	1.10	4.40	0.35	3.10	0.51	1.50	0.19	1.30	0.19	10.3
WR1	11.6	18.1	38.0	4.40	18.0	2.30	0.500	2.40	0.27	1.90	0.35	1.00	0.12	1.00	0.12	6.00
WR2	10.5	16.3	34.0	4.20	18.0	2.10	0.600	2.30	0.23	1.90	0.35	1.00	0.12	1.00	0.15	5.50

Table 7.2: Element content of digested <32μm fractions of environmental samples. Loss on ignition (LOI) at 1000°C. Na, Mg, Al, Si, P, K, Ca, Ti, Mn and Fe determined by ICP-OES, other elements determined by ICP-MS. Elements not measured are marked with "ND" (not determined).

Sample	LOI (%)	Na (ppm)	Mg (ppm)	Al (ppm)	Si (ppm)	P (ppm)	K (ppm)	Ca (ppm)	Sc (ppm)	Ti (ppm)	Mn (ppm)	Fe (ppm)	V (ppm)	
SPK0	12.1	5330	7690	78000	284000	426	16700	5660	14.2	5530	542	34700	113	
SPK1	11.8	4940	8170	81100	283000	466	17400	5710	13.0	5590	561	36200	114	
SPK2	12.0	5640	7530	75300	284000	401	16400	5380	11.9	5560	524	33400	106	
SPK3	11.4	5490	7630	77200	286000	426	16800	5690	10.9	5570	543	33800	105	
SPK4	11.0	4810	8010	79000	277000	458	17200	5700	13.3	5560	541	35700	113	
SPK5	12.2	4890	7840	77300	278000	437	17000	5500	11.6	5510	542	34900	111	
SPK6	11.8	5300	7780	78200	201000	432	17000	5490	16.1	5610	542	34700	112	
Sample	Cr (ppm)	Co (ppm)	Rb (ppm)	Sr (ppm)	Zr (ppm)	Nb (ppm)	Cs (ppm)	Ba (ppm)	Tl (ppm)	Pb (ppm)	Y (ppm)	La (ppm)	Ce (ppm)	
SPK0	95	9.40	91.0	104	106	18.4	6.60	342	0.63	35	18.2	36.1	73	
SPK1	94	9.60	93.0	103	107	18.6	7.50	365	0.70	36	20.4	36.4	74	
SPK2	92	9.00	83.0	96.0	106	16.8	6.70	353	0.76	34	19.0	34.4	72	
SPK3	95	10.4	87.0	111	111	17.8	7.30	347	0.73	35	20.1	35.0	74	
SPK4	95	10.2	89.0	103	97.0	17.7	7.90	358	0.74	34	18.2	37.2	79	
SPK5	93	9.10	84.0	101	107	17.6	7.60	343	0.70	34	19.2	35.1	130	
SPK6	86	9.70	85.0	109	107	17.3	6.80	368	0.84	35	18.2	35.5	610	
Sample	Pr (ppm)	Nd (ppm)	Sm (ppm)	Eu (ppm)	Gd (ppm)	Tb (ppm)	Dy (ppm)	Ho (ppm)	Er (ppm)	Tm (ppm)	Yb (ppm)	Lu (ppm)	Th (ppm)	U (ppm)
SPK0	8.4	35	5.3	1.1	4.7	0.560	4.2	0.70	2.3	0.30	2.1	0.33	10.9	2.1
SPK1	9.2	36	5.9	1.0	4.4	0.550	4.4	0.74	2.1	0.31	2.0	0.27	10.5	2.3
SPK2	8.9	35	4.9	1.2	4.3	0.530	3.8	0.76	2.0	0.27	1.9	0.34	10.0	2.2
SPK3	9.3	37	6.2	1.0	4.5	0.500	4.3	0.77	2.1	0.31	2.2	0.23	10.5	2.1
SPK4	10	40	5.9	0.90	4.9	0.510	4.3	0.82	2.3	0.20	2.0	0.23	10.5	2.3
SPK5	7.9	32	5.5	1.0	4.9	0.550	3.7	0.74	2.2	0.31	2.3	0.31	10.8	2.1
SPK6	7.5	32	5.2	1.1	5.4	0.380	3.7	0.76	2.1	0.23	2.2	0.23	11.3	1.0

Table 7.3: Element content of digested <32 μ m fractions of spiked samples. Loss on ignition (LOI) at 1000°C. Na, Mg, Al, Si, P, K, Ca, Ti, Mn and Fe determined by ICP-OES, other elements determined by ICP-MS.

Sample	Al (ppm)	Si (ppm)	Sc (ppm)	V (ppm)	Cr (ppm)	Fe (ppm)	Co (ppb)	Rb (ppb)	Sr (ppb)	Y (ppb)	Zr (ppb)	Nb (ppb)	Cs (ppb)	Ba (ppb)	La (ppb)	Ce (ppb)
PS2	427	808	0.0587	0.750	0.574	161	63.2	515	338	43.5	191	16.7	48.2	1130	75.0	149
LT1	334	644	0.0398	0.565	0.430	130	27.4	452	274	39.2	128	11.4	53.9	923	49.5	87.8
LT2	101	171	0.0129	0.171	0.116	55.3	11.0	143	28.7	7.30	29.4	8.30	13.1	392	9.10	22.2
WR1	41.0	95.7	0.00730	0.120	0.124	36.0	12.6	66.6	49.3	7.20	47.1	4.80	7.80	410	9.70	22.2
WR2	25.8	54.0	0.00550	0.0949	0.0738	24.0	8.80	34.9	44.6	4.50	21.6	3.40	5.50	267	5.00	12.6
SPK0	371	668	0.0529	0.627	0.510	190	45.0	458	219	52.0	171	22.0	47.4	1110	71.6	143
SPK1	365	653	0.0605	0.617	0.501	187	43.5	451	209	52.1	191	20.2	46.1	1080	67.8	147
SPK2	346	627	0.0590	0.586	0.460	172	40.5	420	187	44.8	181	17.4	43.0	1050	62.5	134
SPK3	301	603	0.0470	0.531	0.406	157	36.4	365	191	46.3	174	18.1	39.3	911	58.1	117
SPK4	332	620	0.0609	0.569	0.451	169	40.2	407	189	45.7	153	20.4	41.6	985	59.5	150
SPK5	333	599	0.0584	0.569	0.460	171	42.4	416	192	48.7	157	18.9	40.5	1000	57.7	388
SPK6	338	617	0.0498	0.572	0.456	169	35.7	420	185	46.1	162	18.4	43.4	975	63.5	2570
Sample	Pr (ppb)	Nd (ppb)	Sm (ppb)	Eu (ppb)	Gd (ppb)	Tb (ppb)	Dy (ppb)	Ho (ppb)	Er (ppb)	Tm (ppb)	Yb (ppb)	Lu (ppb)	Tl (ppb)	Pb (ppb)	Th (ppb)	U (ppb)
PS2	14.8	57.1	10	2.1	9.5	1.4	8.1	1.6	5.3	0.80	5.7	0.70	3.9	183	31.0	3.90
LT1	10.3	35.1	6.7	1.5	6.9	1.1	6.9	1.3	3.6	0.50	3.8	0.50	3.0	100	24.6	3.10
LT2	1.90	8.70	1.6	0.30	1.6	0.30	1.5	0.30	1.0	0.10	0.60	0.20	1.2	131	7.30	1.40
WR1	2.20	8.80	1.2	0.30	1.3	0.30	1.3	0.30	0.60	0.20	0.80	0.0	0.70	88.8	5.70	0.600
WR2	1.60	6.40	0.80	0.20	1.0	0.20	1.0	0.20	0.30	0.0	0.30	0.10	0.40	46.6	2.70	0.500
SPK0	16.5	55.3	12	2.2	10	1.7	11	2.1	5.6	0.90	5.1	0.70	3.3	119	37.1	4.50
SPK1	13.7	55.7	11	2.6	10	1.7	9.9	2.2	5.8	0.90	5.3	0.70	3.5	118	37.3	4.60
SPK2	12.9	53.8	11	2.2	10	1.4	9.1	1.8	4.8	0.90	5.1	0.60	3.1	101	32.2	3.60
SPK3	13.9	49.5	9.5	2.5	9.9	1.6	8.2	2.1	5.3	0.90	4.9	0.80	2.9	101	32.6	3.50
SPK4	13.5	55.2	11	2.0	10	1.4	9.3	1.8	4.7	0.80	5.0	0.60	3.1	107	33.7	3.80
SPK5	12.2	50.1	9.5	1.9	9.5	1.6	9.3	1.9	5.7	0.80	5.0	0.70	3.1	105	32.8	4.00
SPK6	13.2	49.0	10	2.3	13	1.5	9.4	1.9	4.9	0.80	5.0	0.60	3.0	97.1	31.8	3.50

Table 7.4: Element content of colloidal extracts (mass per volume). All elements determined by ICP-MS, except for Si (ICP-OES).

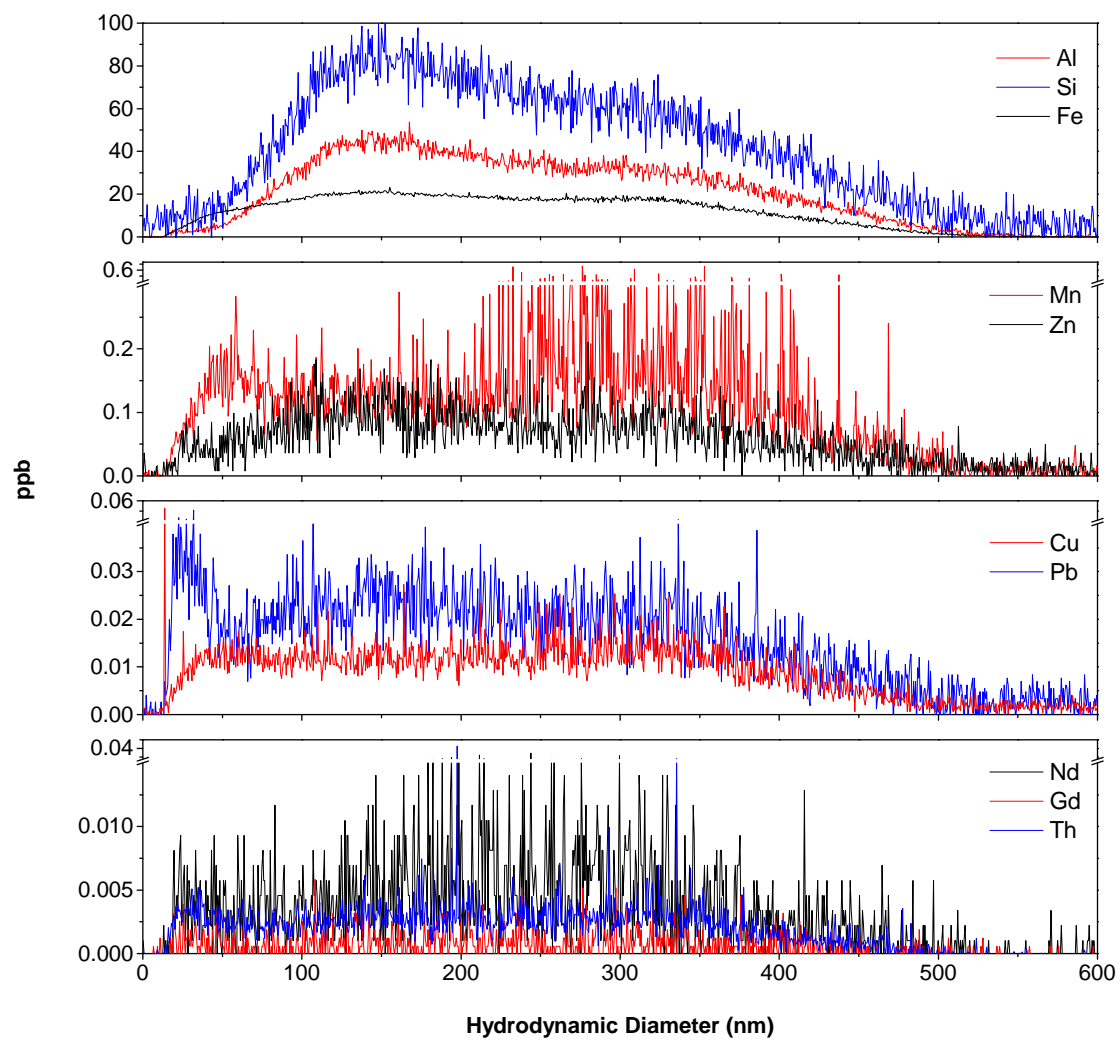


Figure 7.1: A4F-ICP-MS data of colloid sample SPK0 for multiple elements.

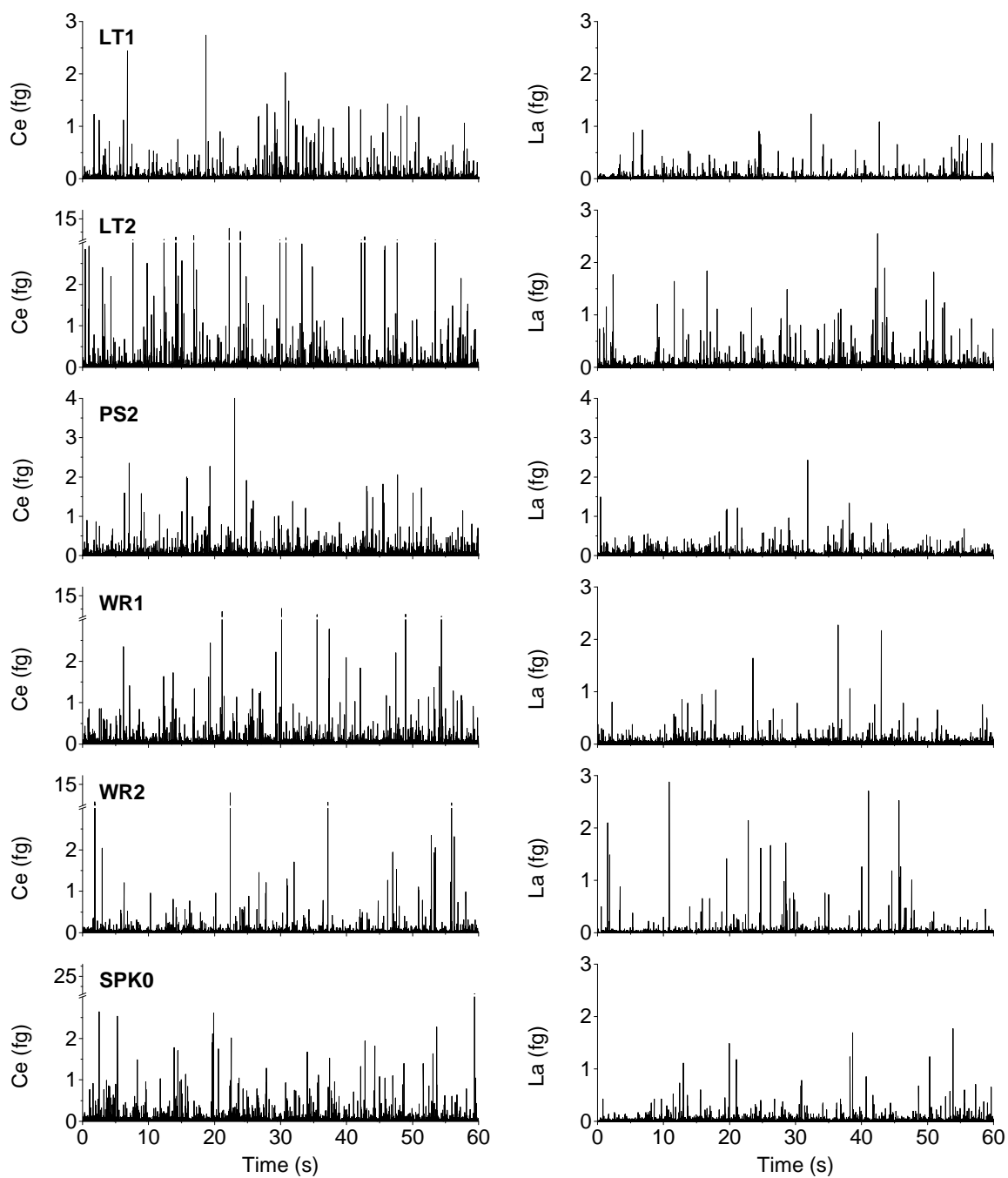


Figure 7.2: Single particle ICP-MS fractograms of natural and road run-off colloid extracts. All samples were measured $1000\times$ diluted.

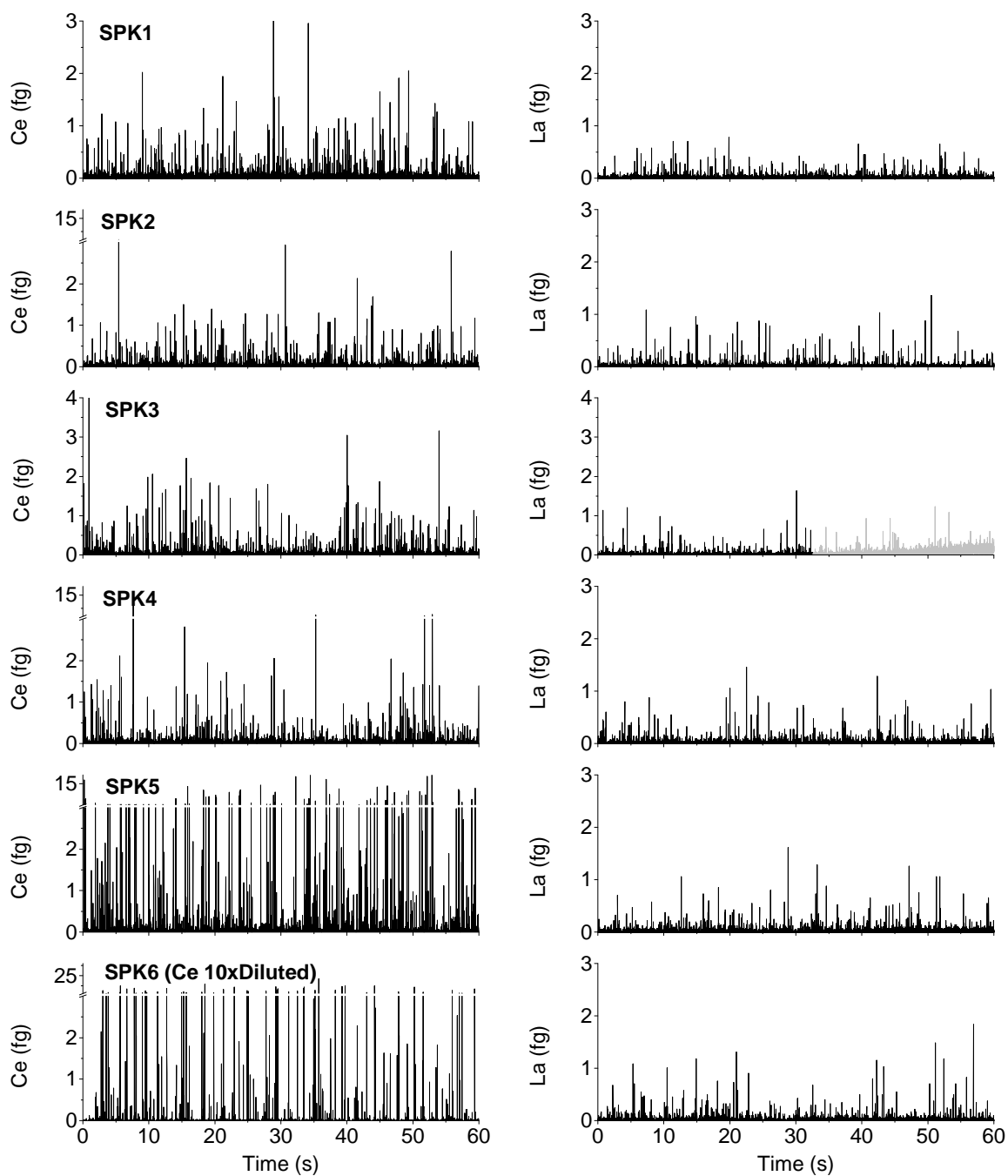


Figure 7.3: Single particle ICP-MS fractograms of spiked colloid samples. All samples were measured $1000\times$ diluted, except for Ce SPK6 ($10000\times$ diluted). The La measurement of SPK3 shows a drift from 30–60 s which was not used for particle counting analysis.

7.3 Eidesstattliche Erklärung

Ich erkläre hiermit an Eides statt, dass ich die vorliegende Arbeit selbstständig und ohne Benutzung anderer als der angegebenen Hilfsmittel angefertigt habe.

Die aus fremden Quellen direkt oder indirekt übernommenen Gedanken sind als solche kenntlich gemacht.

Die Arbeit wurde bisher in gleicher oder ähnlicher Form keiner anderen Prüfungskommission vorgelegt und auch nicht veröffentlicht.

Wien, am 23.03.2015

Willi Fabienke

7.4 Curriculum Vitae

Willi Fabienke

Personal Information

Name Willi Fabienke

Citizenship Germany

Education

2012–2015 M.Sc., Earth Sciences, University of Vienna

2009–2012 B.Sc., Earth Sciences, University of Vienna

2008 University-entrance diploma

2000–2008 Secondary Education, BG/BRG Stockerau

March 23, 2015